Entry dynamics and acoustics/infrasonic/seismic analysis for the Neuschwanstein meteorite fall

D. O. REVELLE,[1]* P. G. BROWN,[2] and P. SPURNÝ[3]

[1]Los Alamos National Laboratory, P.O. Box 1663, MS D401, Los Alamos, New Mexico 87545, USA
[2]Canada Research Chair in Meteor Science, Department of Physics and Astronomy,
University of Western Ontario, London, Ontario N6A 3K7, Canada
[3]Ondrejov Observatory, Astronomical Institute of the Academy of Sciences of the Czech Republic, 251 65 Ondrejov, Czech Republic
*Corresponding author. E-mail: revelle@lanl.gov

Abstract–We have analyzed several types of data associated with the well-documented fall of the Neuschwanstein meteorites on April 6, 2002 (a total of three meteorites have been recovered). This includes ground-based photographic and radiometer data as well as infrasound and seismic data from this very significant bolide event (Spurný et al. 2002, 2003). We have also used these data to model the entry of Neuschwanstein, including the expected dynamics, energetics, panchromatic luminosity, and associated fragmentation effects. In addition, we have calculated the differential efficiency of acoustical waves for Neuschwanstein and used these values to compare against the efficiency calculated using available ground-based infrasound data. This new numerical technique has allowed the source height to be determined independent of ray tracing solutions. We have also carried out theoretical ray tracing for a moving point source (not strictly a cylindrical line emission) and for an infinite speed line source. In addition, we have determined the ray turning heights as a function of the source height for both initially upward and downward propagating rays, independent of the explicit ray tracing (detailed propagation path) programs. These results all agree on the origins of the acoustic emission and explicit source heights for Neuschwanstein for the strongest infrasonic signals. Calculated source energies using more than four different independent approaches agree that Neuschwanstein was certainly <500 kg in initial mass, given the initial velocity of 20.95 km/s, resulting in an initial source energy ≤0.0157–0.0276 kt TNT equivalent (4.185×10^{12} J). Local source energies at the calculated infrasonic/seismic source altitudes are up to two orders of magnitude smaller than this initial source energy.

INTRODUCTION

The Neuschwanstein meteorite fall occurred at 20:20 UT on April 6, 2002. The bright fireball that accompanied the meteorite fall was widely observed in southern Germany, Austria, and the Czech Republic. Of particular interest are the photographic recordings of the fireball made from several German, Czech, and Austrian stations of the European fireball network (Spurný et al. 2002) that permit accurate computation of the fireball trajectory and pre-atmospheric orbit. In addition to these data, high resolution, radiometric recordings of the fireball brightness were made at three stations, allowing precise timing and light curve reconstruction.

While recovery of a meteorite with a known orbit is a significant observation in and of itself—this has been

accomplished only six times before (cf. Borovička et al. 2003a)—the orbit of the Neuschwanstein meteorite is exceptional in that it is identical to the Pribram meteorite fall of April 7, 1959 (Spurný et al. 2002). This unusual situation is further complicated by the fact that the Neuschwanstein meteorite is an EL chondrite, unlike the Pribram meteorite, which was an H chondrite. These data strongly support the contention of Halliday et al. (1990) concerning the existence of asteroidal-meteorite streams but poses questions regarding the origin of such streams given the dissimilar chemical character of these two dynamically related bodies.

As part of the multi-instrumental study of the fall of the Neuschwanstein meteorite, recordings of the airwave associated with the fireball have been examined. These include infrasonic recordings from Germany and the Netherlands as well as seismically coupled airwave signatures

on nine seismographs in the immediate region of the fireball endpoint. These data permit detailed reconstruction of many aspects of the shock production associated with the Neuschwanstein fireball, as the precise path in the atmosphere can be combined with acoustic propagation modeling to disentangle fragmentation and acoustic radiation patterns. In particular, by examining infrasound and seismically coupled airwave data in conjunction with modeling, we hope to determine the source altitude for the acoustic signal observed at each station and measure the extent and location of fragmentation points along the trajectory and, therefore, set limits on the deviation (if any) of the acoustic radiation pattern from the standard bolide cylindrical line source model (cf. ReVelle 1976) for such fragmentation points. Additionally, the propagation channels for each portion of the infrasound signal for proximal stations can be determined, and estimates for the total energy of the fireball can be made based on these recorded airwave data.

DETAILED ENTRY DYNAMICAL SIMULATIONS FOR NEUSCHWANSTEIN

Starting from flight data given in Spurný et al. (2002, 2003) and using a newly developed FORTRAN computer code (ReVelle 2001, 2002a, b), we have been able to evaluate the detailed entry behavior of Neuschwanstein and compute the corresponding dynamics, energetics, expected fragmentation effects, and also make quantitative luminosity predictions (over the panchromatic pass-band region from 360–675 nm) for the bolide. The full details of this code will be reported shortly, including discussions of newly developed concepts that separate the traditional single-body entry dynamics treatment from a more thorough analysis including the fragmentation-dominated flow regime.

We have used the following input values for the Neuschwanstein meteorite fall, as largely constrained from the photographic flight data: initial radius = 0.33 m, with a corresponding entry velocity = 20.95 km/s at an entry angle measured from the zenith of 40.25°. We assumed a maximum number of eight fragments for a body (based on observations in Spurný et al. 2002, 2003) the shape of which was assumed to be spherical (S_f = 1.209, the shape factor ≡ frontal cross-sectional area/volume$^{2/3}$). For μ, the shape change factor = 2/3 (which corresponds to a self-similar solution with no shape change allowed), and the corresponding D or energetics parameter of ReVelle = 4.605 (corresponding to 99% of the original kinetic energy available at the "top" of the atmosphere having been depleted at the end of the visible trajectory). The ablation parameter, σ, is a full function of height/time in all of these simulations, and a nominal, volume-weighted porosity was assumed to be equal to 5% (though some trial values as large as 10% were also used). However, values of μ as small as 0.10 (ReVelle and Ceplecha 2001b) did not greatly modify the results given above.

These calculations were accomplished entirely in Cartesian coordinates (as the entry angle was greater than 10° upward from the horizon) using a hydrostatic, perfectly stratified (along the vertical axis), steady state model atmosphere that was appropriately modified to correspond to the typical properties of a U.S. Standard Atmosphere (indicative of a summer situation in middle latitudes). Both the ambient atmospheric pressure and the vertical air density profiles have been calculated using this atmospheric modeling assumption for all entry model computations.

Finally, we have allowed the temporal/spatial wake behavior of all of the fragments to correspond to a state of collective wake action of all of the fragments (one of three available options in the computer code) such that:

1. Either the particles are put into the wake and permanently "lost" from a luminosity and deceleration standpoint, i.e., they always remain in the wake behind the original leading fragment;
2. The fragments are put into the wake and brought back forward to increase the frontal area and effect both the luminosity and the deceleration after a short time delay that is a function of the bolide's speed; or
3. There is also the possibility of an intermediate condition that accomplishes the last option in a quasi-periodic manner. This has not yet been fully implemented in our code.

The 5% porosity value assumed in the list above is most likely an upper limit to the "true" value for this bolide, especially given its true nature as an EL chondrite (Spurný et al. 2002). In general, as both the volume-weighted porosity and the final number of fragments are allowed to increase, the predicted luminosity of a given bolide will also increase but for differing reasons. Thus, we have varied both of these fundamental parameters independently while maintaining various upper limits on each one separately to determine sensitivities in the final result. This is discussed further below. Figures 1–5 give the results for the predicted values of:

- panchromatic stellar magnitude versus time;
- mass versus time;
- panchromatic luminosity (watts/steradian) versus time;
- height versus velocity;
- ablation parameter versus time.

The observed peak stellar magnitude (or equivalently, the predicted panchromatic luminosity in watts/steradian) for this combination of parameters agrees quite well with the maximum value proposed by Spurný et al. (2002, 2003). The predicted mass behavior (initial mass and final mass, etc.) also agrees well with the observations, as does the final velocity of the meteorites just before dark-flight began. Table 1 summarizes many of our modeling results for Neuschwanstein. The final entry dynamics initial source energy estimate has been found to agree quite well with those found using other techniques (see below).
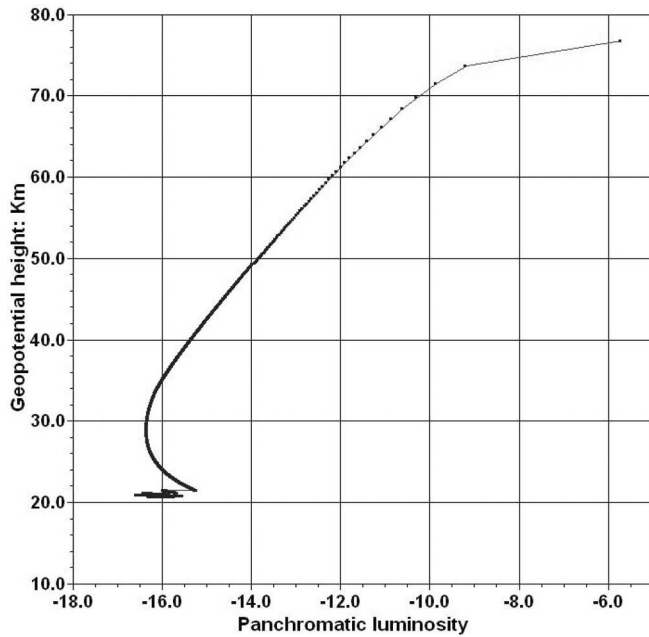
Fig. 1. Predicted panchromatic stellar magnitude versus time (sec) for Neuschwanstein.
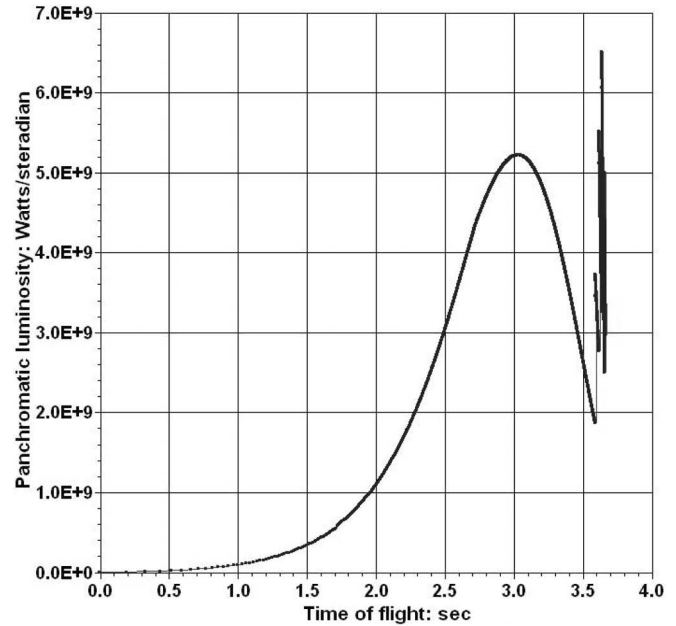

Fig. 3. Predicted panchromatic luminosity (watts/steradian) versus time (sec) for Neuschwanstein.
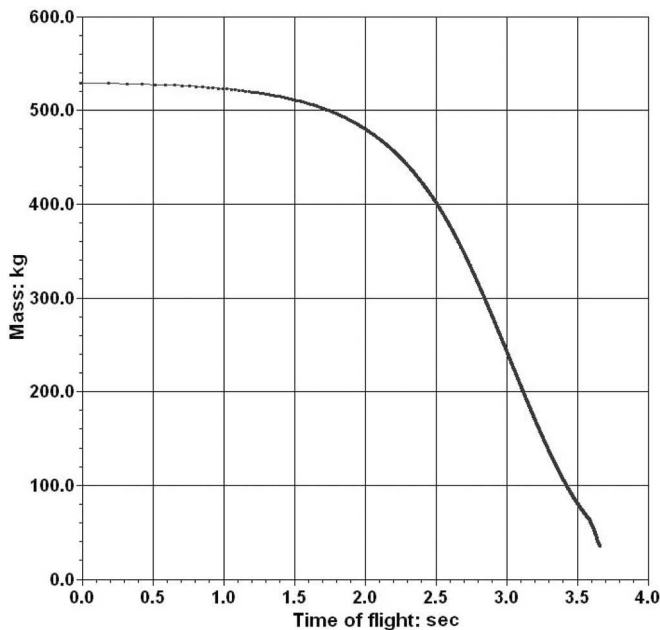

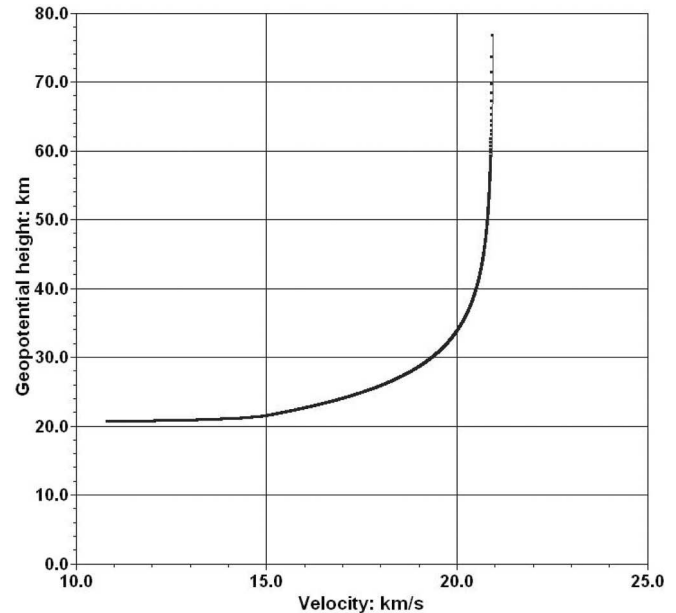Fig. 2. Predicted mass (kg) versus time (sec) for Neuschwanstein.

Fig. 4. Predicted height (km) versus velocity (km/s) for Neuschwanstein.

Infrasonic Recordings

Infrasound is that portion of the atmospheric acoustic wave spectrum below ~20 Hz (sub-audible) and above the natural oscillation Brunt-Vaisalla frequency of the atmosphere ($>$~0.02 s^{-1} in angular frequency or $>$~3.2 × 10^{-3} Hz or $<$~311 sec in period) below which internal atmospheric gravity waves with generally sub-acoustic propagation velocities dominate (cf. Beer 1974). Any mechanism that generates coherent motion of the atmosphere over large spatial scales ($>$10s to 100s of m) and/or at high velocities can radiate energy in the infrasonic regime. If the horizontal scale of the source is comparable to or exceeds the local pressure (or density) scale height, emissions tend to be concentrated at gravity wave frequencies rather than in the infrasonic regime, as in the case of the Tunguska event of June 30, 1908. Of particular importance to its utility in long-range detection, the attenuation of infrasonic waves in the lower atmosphere is

very small—acoustic radiation with frequencies below a few Hz can result in detections at 100s to many 1000s of km, depending on the initial source energy and altitude, atmospheric turbulence levels, and winds.

The long-distance detection of infrasound from fireballs has been used previously to determine influx rates for m-sized bodies (ReVelle 1997, 2002) and for the estimation of bolide energies (ReVelle 1976). Recently, infrasound records have been combined with satellite data to estimate bolide source energies, luminous efficiencies, and to calibrate influx rates observed by satellite systems (Brown et al. 2002b), while multi-
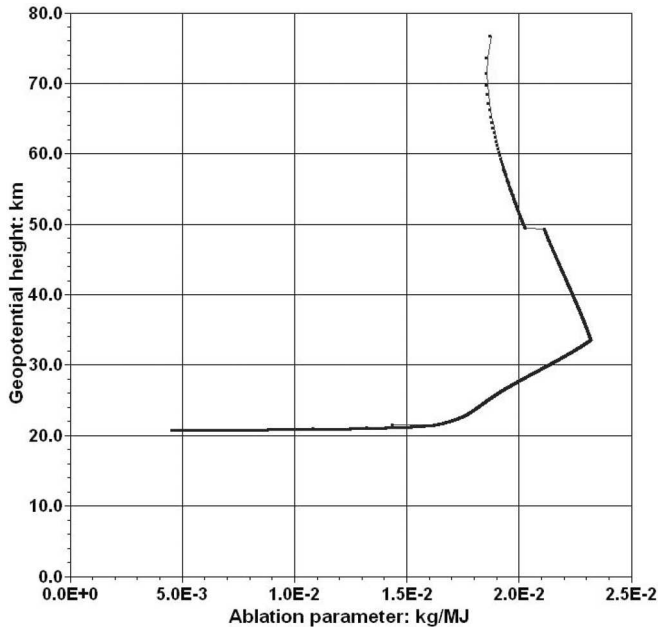

Fig. 5. Predicted ablation parameter, σ, (in kg/MJ) versus time (sec) for Neuschwanstein.

station recordings have been employed for bolide geolocation (Brown et al. 2002c). A recent analysis of the Morávka meteorite fall (Borovička et al. 2003a; Brown et al. 2003) has placed some limits on characteristics of the shock wave source at the fireball from both the ballistic wave and fragmentation events, suggesting that the deviation of the ray normals for the fragmentation events may be as much as 30° beyond that expected from a purely cylindrical line source blast.

The infrasonic signals from the Neuschwanstein fireball were recorded in Freyung, Germany by station FREYUNG (IS26) (13.7131° E, 48.8516° N, elevation above sea level, h = 1111 m). This station is part of the International Monitoring System (IMS) of the Comprehensive Test Ban Treaty (CTBT) infrasound array located at a distance of 256 km from the point of fireball maximum light (see Spurný et al. 2002). The signals detected at the five low frequency microphones of the IS26 array are shown in Fig. 9. Weak airwaves from the event may also have been detected at the Deelen Infrasound array in the Netherlands (Evers and Haak 2001) at a range of 622 km. IS26 recorded the airwave arrival from the fireball beginning 820 sec after the fireball (20:33:53 UT) and ceasing approximately 100 sec later at 20:35:33 UT.

Using the signal from all five elements and applying standard beam-forming techniques to search for maximum cross-correlation within 20 sec bin windows (cf. Evers and Haak 2001), the azimuth of the peak signal cross-correlation and the value of the peak cross-correlation are indicated in Fig. 10.

Figures 9 and 10 clearly show that the fireball airwave consists of two distinct portions: an early, impulsive arrival near 820 sec, lasting <10 sec and composed of high frequency energy (>1 Hz), and a larger amplitude signal beginning 1 min later, consisting of several sub-maxima, lasting longer, and having a comparably higher frequency. It is notable that,

Table 1. Summary of entry dynamics: Findings for Neuschwanstein.

Neuschwanstein meteorite fall results	Parameters
Initial source energy	0.0157 kt (1 kt = 4.185×10^{12} J)
Initial source energy: entry modeling results	0.0276 kt (1 kt = 4.185×10^{12} J); see below
Initial mass: (kg) estimate by Spurný et al. (2002, 2003)	300 ± 100 kg
Initial radius and mass: (kg) entry modeling	0.33 m, 529.1 kg (0.30 m, 397.5 kg if the total number of fragments is 16–50; see below)
Final mass: (kg) independent estimate	≥6.22 kg (1.63, 1.75, and 2.84 kg with a total estimate on the ground = 20 kg). These three meteorites were recovered in very rugged terrain, so it is unlikely that more will be recovered.
Final mass: (kg) entry modeling	35.5 kg (28.4 kg for 16–50 total fragments, an initial radius = 0.30 m, an initial mass = 397.5 kg, and an initial source energy = 0.0208 kt)
Volume weighted porosity (%)	0–10% (<5% is the nominal best-fit value)
Total number of fragments assumed (nominal): assuming 16–50 fragments with a smaller initial radius produce even better agreement with the results of Spurný et al. (2002, 2003).	8; this could not be reliably determined from the photographs at the closest German EFN station, the optics of which are not comparable to the standard fish-eye lens used at other stations.
Stagnation pressure at significant break-up: observed	4.6 MPa
Stagnation pressure at significant break-up: model value	2.90 MPa
Semi-empirical, maximum luminous efficiency: differential value	6.9%

within the second wavetrain, the azimuth bearings for the peak correlation move systematically to lower azimuths beginning near 234° and shifting to ~225° some 40 sec after the peak amplitude is reached (see Fig. 10). The peak amplitude for the first wavetrain (hereafter, wavetrain a) is ~1.55 ± 0.33 Pa, while that for the second (wavetrain b) is

5.36 ± 1.94 Pa. While the magnitude of the cross-correlation falls below the general background level for this bandpass and window binning size, the near steady azimuth values from 810–950 sec indicate substantially longer signal durations than the cross-correlation alone would suggest. Indeed, using other bandpass/window binning combinations produces significant cross-correlations above background over this entire interval. The signal energy between wavetrains a and b
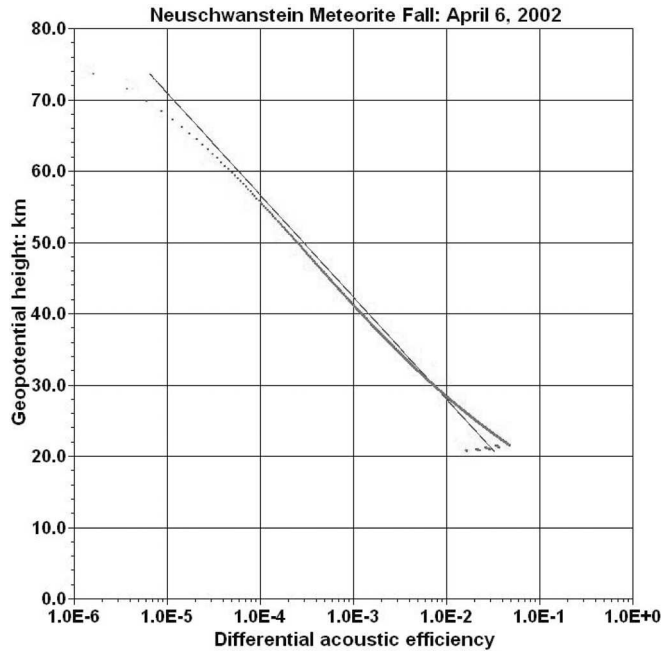

Fig. 6. Predicted differential acoustic efficiency values and the least-squares curve fit used in this study versus height (km) for Neuschwanstein.
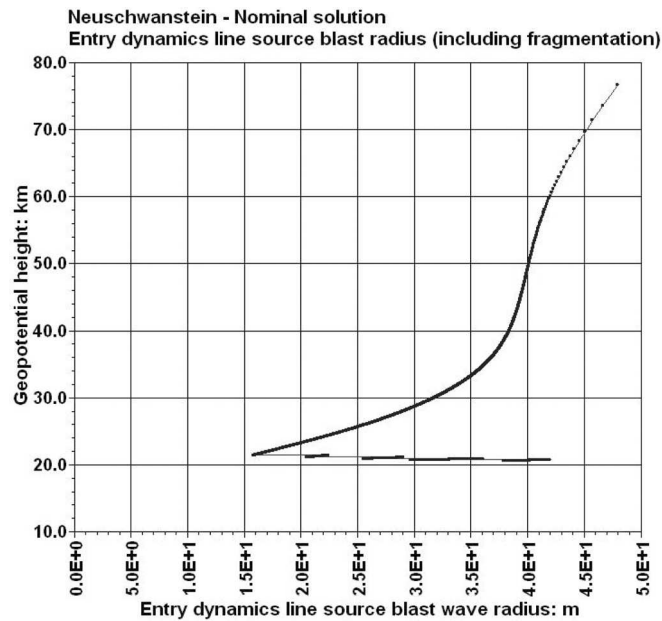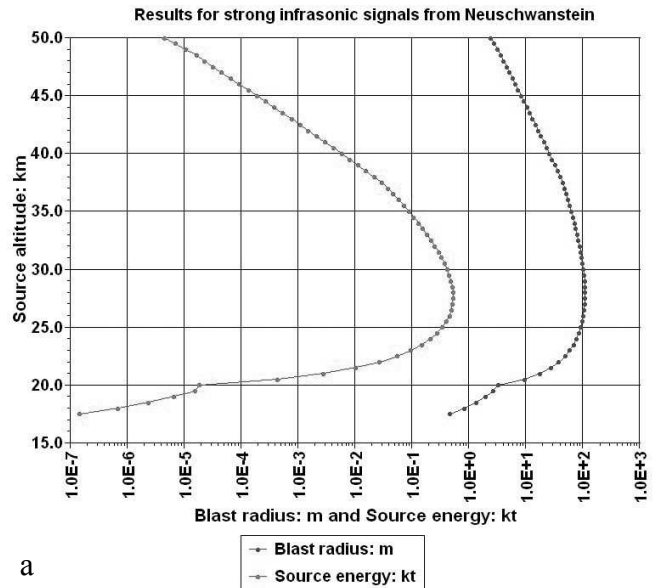

Fig. 7. Predicted entry dynamics line source blast wave relaxation radius (including fragmentation effects) versus height (km) for Neuschwanstein.
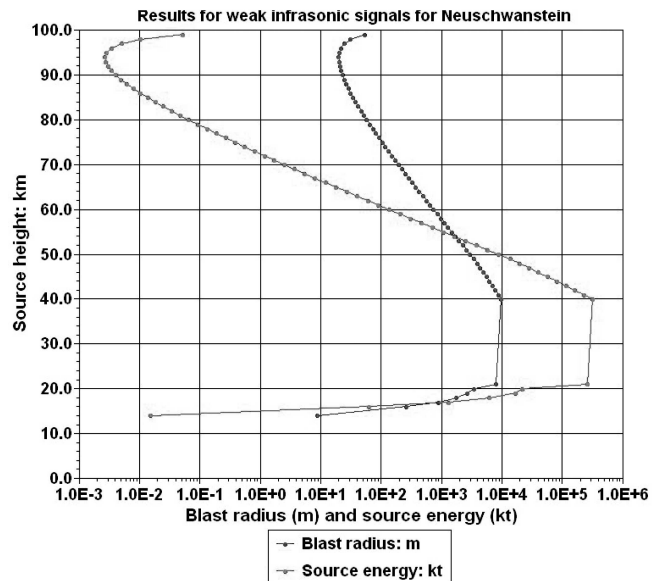

a

Fig. 8. Numerically predicted line source blast radius and concomitant source energy as a function of height simultaneously using the entry dynamics values of the theoretical differential acoustic efficiency, modeled mass, modeled velocity, and entry angle and the observed infrasonic pressure amplitude at the ground; strong infrasound results using a search altitude step = 0.50 km (a) and weak infrasound results using a search altitude step = 1.0 km (b). See text for an explanation of the new technique.
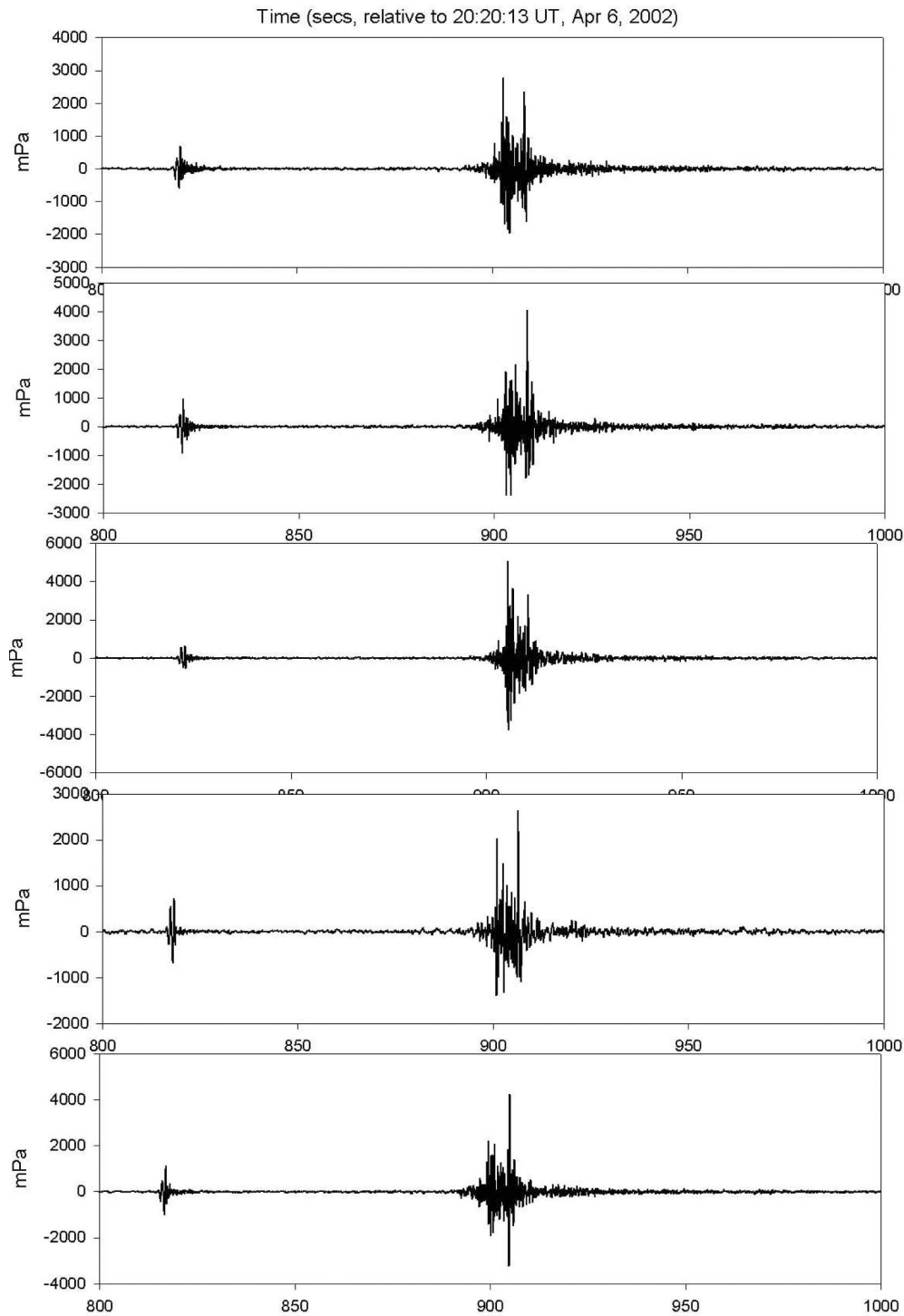
Fig. 9. The recorded infrasound signal on all five channels at Freyung for the Neuschwanstein fireball. Note that these waveforms have been high-passed above 0.40 Hz to most clearly define the fireball signal. The time is relative to 20:20:13 UT on April 6, 2002.

and the signal after 920 sec in wavetrain b are of minor amplitude and may indicate scattering/diffracted acoustic energy or could be returns from atmospheric paths extending to higher altitudes (and, thus, suffering greater attenuation).

The examination of the airwave's apparent trace velocity (a measure of the signal's apparent velocity of travel from one microphone to the next; the steeper the airwave arrival, the higher the trace velocities) shows no significant trend across the signal—these values all lie near 0.33 ± 0.02 km/s, implying fairly shallow local arrivals.

To link these observed infrasonic data with the Neuschwanstein fireball, we use the accurate trajectory
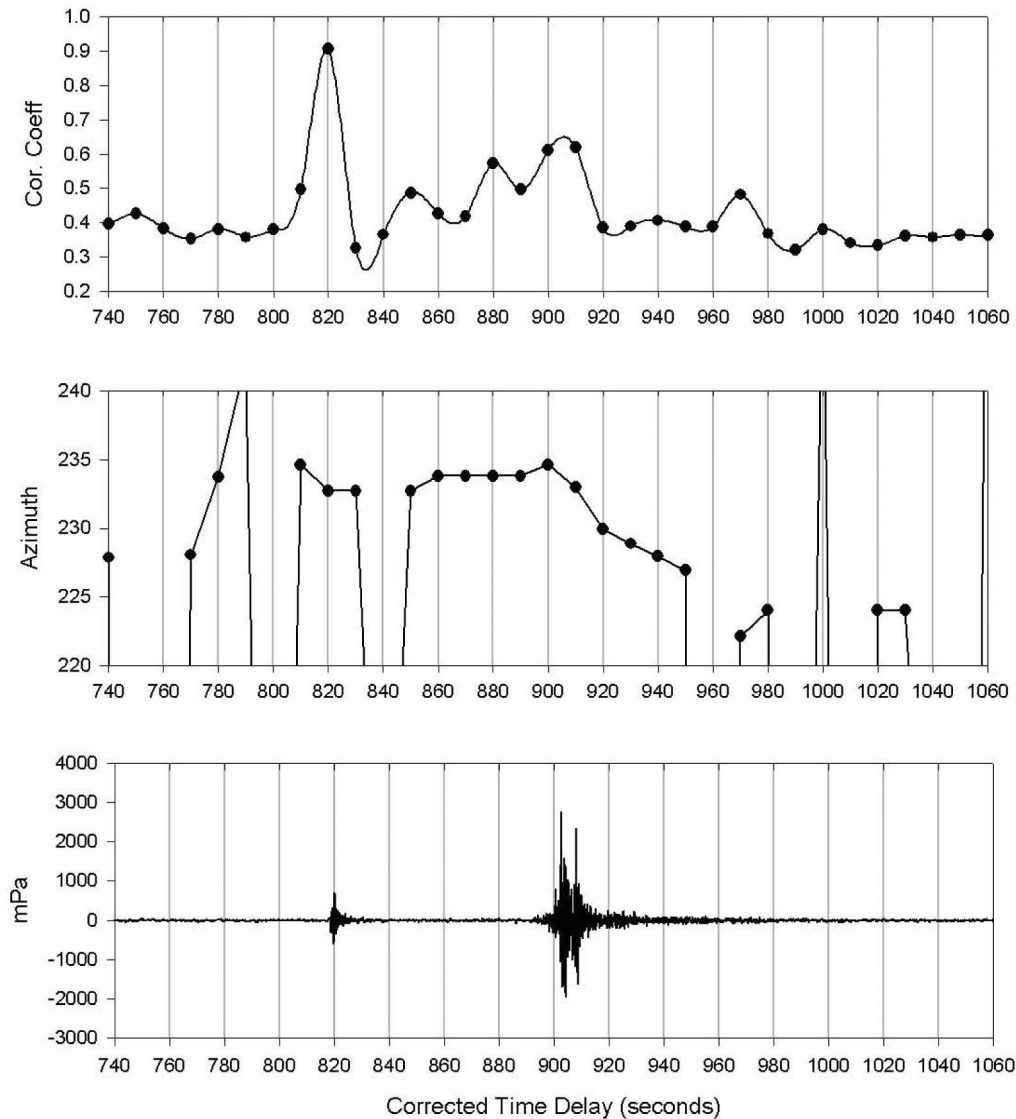
Fig. 10. The maximum correlation coefficient during the time centered around the Neuschwanstein fireball signal at Freyung (top). Cross-correlation windows of 20 sec (with 50% overlap per window) are used to define individual measurements of cross-correlation. The background cross-correlation in this frequency bandpass (0.5–8 Hz) is 0.39 ± 0.02. The associated azimuth to maximum cross-correlation is also shown (middle). The amplitude for channel 1 is also shown at the bottom for comparison.

information together with a numerical acoustic ray tracing code to compare model values for arrival angles and timing with those expected for moving point sources and later for ideal line (infinite speed) and modified line sources (finite speed compared to the local sound speed) distributed along the trail.

Acoustic Numerical Ray Modeling (Moving Point Source Model)

To simulate acoustic production from the Neuschwanstein fireball, we first treat a large number of individual points along the fireball path, assuming each moving point to be a potential producer of acoustic radiation.

Briefly, the modeling procedure involved shooting rays from each point along the trajectory below 40 km in the direction of Freyung but with a wide range of elevation angles. The computer code used in this effort is called InfraMap (BBN 2000). The rays were allowed to propagate through a steady state, range-independent model atmosphere (MSIS-E: mass spectrometer and incoherent scatter model and the horizontal wind model [HWM]; see below for a description of these models).

We followed the complete acoustic path for each ray to determine the delay time and arrival direction at the receiver of those rays passing within 10 km (horizontally or vertically) of the receiver array at Freyung. To model these acoustic arrivals, we made use of the radiosonde data from Munich, Germany

(~70 km north-northeast from the fireball endpoint) taken at 18 UT on April 6, 2002 to define the temperature and wind field up to 32 km in altitude. Above 32 km in altitude, we merged these radiosonde data with the MSIS-E model to produce the temperature profile (cf. Picone et al. 1997) up to a height of 140 km, inputting the appropriate geomagnetic indices for April 6, 2002 (which can significantly affect the atmospheric temperature and, thus, the local sound speed at heights above ~100 km). We note that the MSIS-E temperatures below 32 km were virtually indistinguishable from those of the radiosonde, except in the lower 3–4 km near the ground, i.e., in the atmospheric boundary layer. The wind field above 32 km was approximated using the HWM (Hedin et al. 1996). The wind field and temperature profiles used are shown in Figs. 11a and 11b. This numerical model has also been used previously for interpreting infrasonic data measured for the Morávka fireball (see Brown et al. [2003] for more details).

The results from these model calculations are shown in

Figs. 12–13. Each point in these simulations represents a single height corresponding to the measured shutter break positions along the fireball path as described in Spurný et al. (2003). Figure 12 shows the time delay for the arrival of rays at Freyung as a function of the source height along the fireball path. The time delay includes both the propagation time and a correction for the source generation time due to the finite velocity of the fireball. Figure 13 shows the delay time as a function of the source height along the fireball path and the launch elevation (relative to the horizontal) for rays reaching Freyung as a function of source height. Based on the maximum height reached by the rays, the type of ray path (stratospheric or thermospheric) is given in these figures.

From these figures, it is immediately apparent that the main arrival (wavetrain b) is generated in the lowest portion of the fireball path, between 16–22 km, centered in the vicinity of the brightest portion of the fireball trajectory. In contrast, the
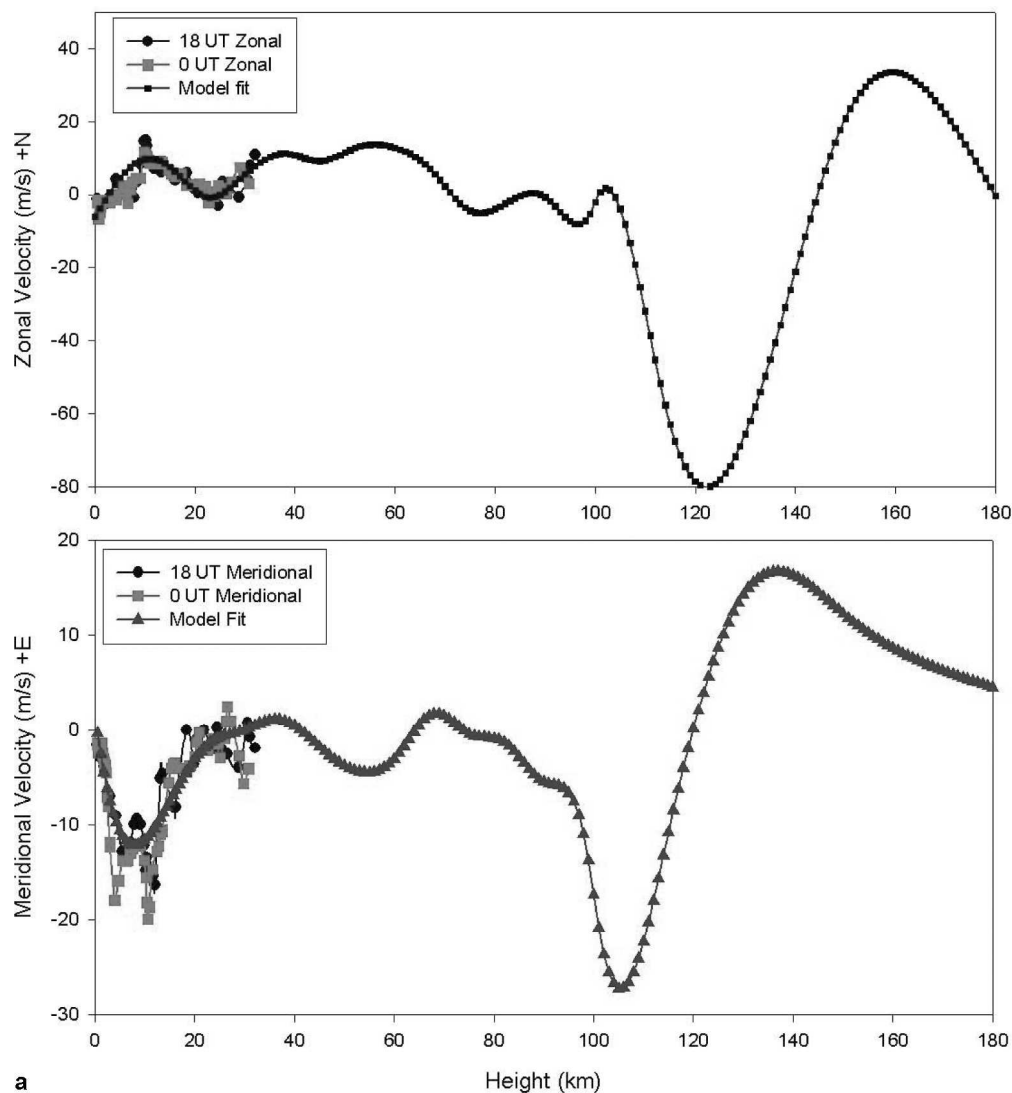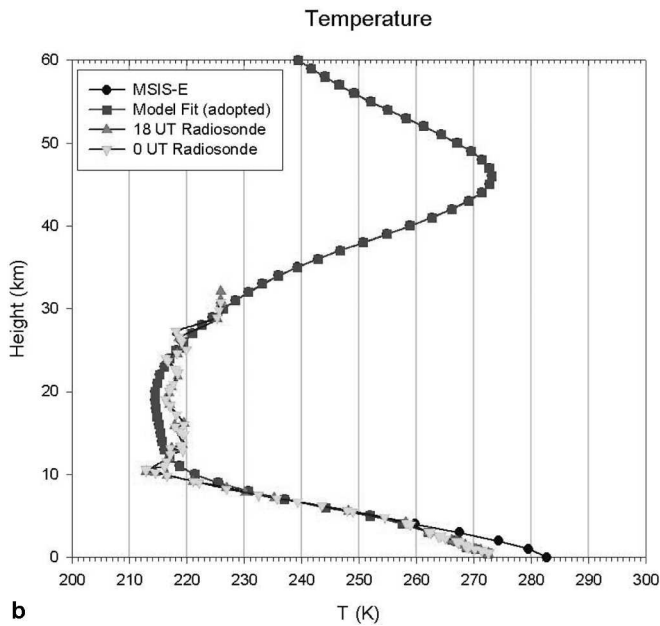

Fig. 11. Wind profile (a) used in numerical ray modeling and comparison to radiosonde data taken near the time of the event.

b

Fig. 11. *Continued.* Temperature (b) used in numerical ray modeling and comparison to radiosonde data taken near the time of the event.

first arrival (wavetrain a) appears to be generated at a height of 30–32 km, which is well before the main detonation.

To independently confirm this interpretation, the apparent arrival azimuth for each modeled ray at Freyung as a function of both height and the corrected delay time is given in Fig. 14. The observed azimuths at Freyung at the time of maximum amplitude for each wavetrain are also shown in the figure. It is clear that the later wavetrain b is a stratospheric arrival emanating from almost precisely the brightest segment of the fireball trail. Similarly, wavetrain a is generated from an altitude of 31 ± 1 km.

To ascertain the probable source mechanisms involved for both wavetrains, we have plotted in Fig. 15a the launch azimuth for rays reaching Freyung from all heights along the fireball path as a function of the ray launch elevation. For a line source blast wave source model, which approximates well the acoustic radiation expected from a non-fragmenting fireball (cf. ReVelle 1976), the rays are launched perpendicular to the fireball path. The locus of the azimuth and of the altitude pairs fulfilling this condition for Neuschwanstein are indicated by the dark line in Fig. 15a. Comparison of this result with that given in Fig. 13 indicates
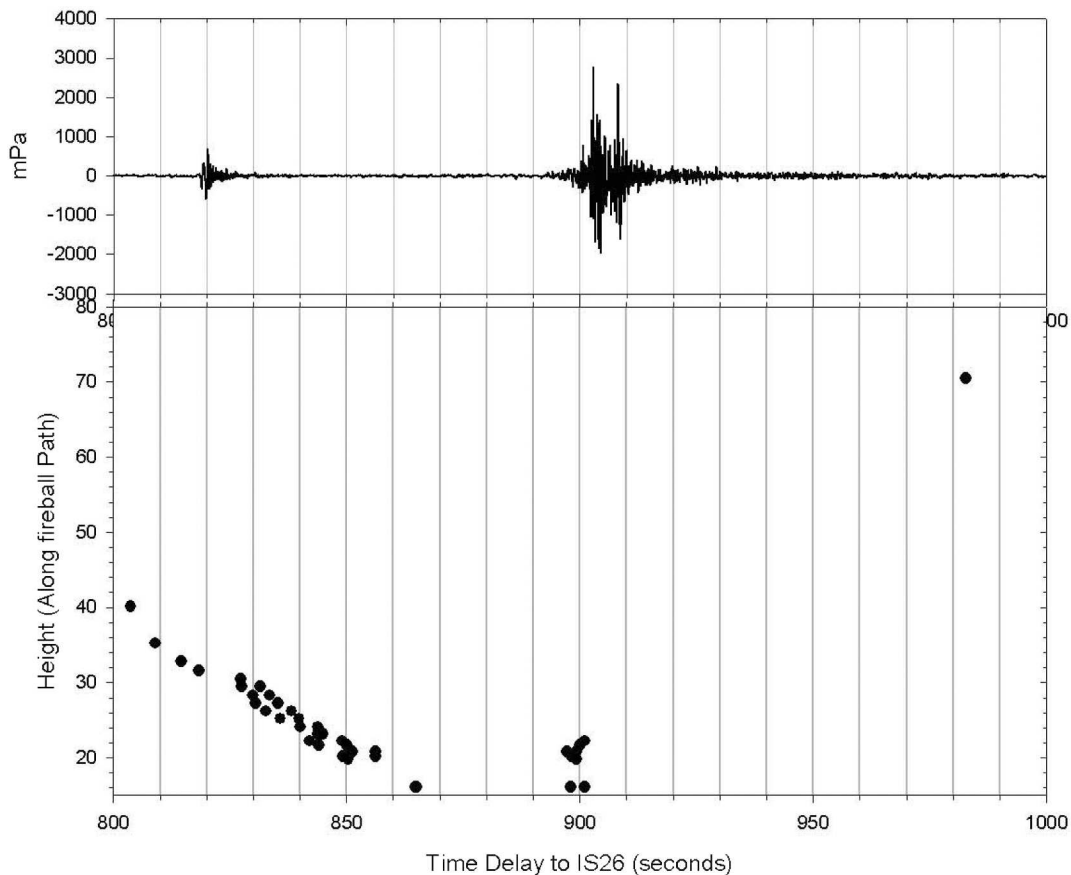

Fig. 12. Source generation heights in km at measured shutter-break points along the fireball entry trajectory as a function of modeled arrival times at IS26 (bottom).
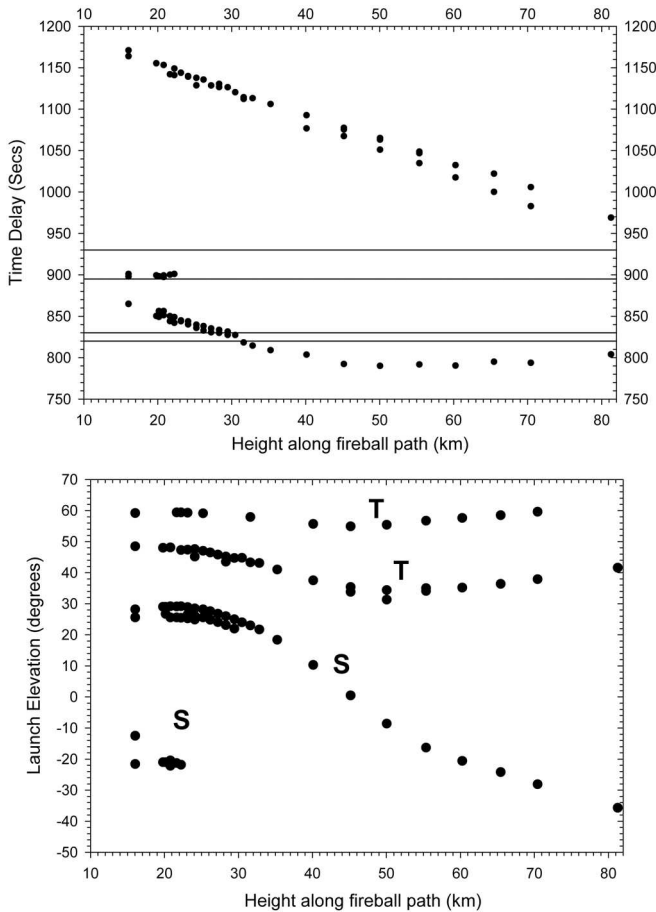
Fig. 13. Ray arrival time delays as a function of generation height (the lines show the extent of significant signal from wavetrains a and b) (top). Ray launch elevation as a function of height along the fireball path (bottom), where T denotes thermospheric returns and S denotes stratospheric returns.
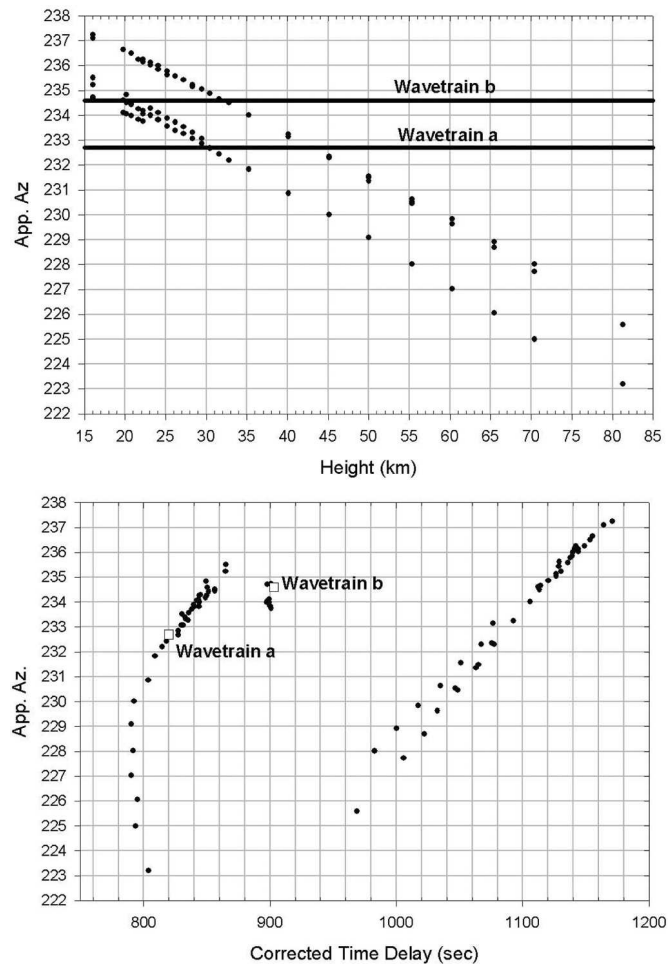

Fig. 14. The apparent azimuth of arrival for modeled rays at Freyung as a function of the source height along the fireball path (top). The observed azimuths of peak cross-correlation at maximum amplitude are also shown for each wavetrain. The apparent arrival azimuth as a function of corrected time delay for ray arrivals at IS26 (bottom). The observed values for wavetrain a and b are shown as open squares.

that the main arrival (wavetrain b) is produced by stratospheric rays that radiate along the cylindrical line source airwave "path." These are geometrically ideally suited to be produced at the fireball source and recorded at Freyung. The reason that these observed rays are so close to being perpendicular in the precise source region where fragmentation occurs is not clear, but this is what we have been able to determine from these calculations.

In contrast, the acoustic paths from an altitude of 31 ± 1 km that are responsible for wavetrain a are launched at upward angles near 23° from the horizontal—this is 33° from perpendicular to the fireball path. The most straightforward interpretation would be that this represents a major fragmentation point for the fireball, as such events are expected to produce quasi-spherical acoustic radiation from a rapidly moving source (cf. Brown et al. 2003).

Line Source and Modified Line Source Ray Tracing Efforts

To compliment the above analysis, we also make use of a recently developed ray tracing code that can be run in either of two respective limits: a) an infinite speed line source mode (with respect to the local adiabatic thermodynamic sound speed at any height); or b) a modified line source mode using the finite speed of the bolide with respect to the local adiabatic thermodynamic sound speed (with this speed ratio held constant at all altitudes).

Both options of the code were used using the identical model atmosphere as above for the moving point source ray tracing efforts to identify various possibilities for ray paths from the bolide for propagation to IS26 (the Freyung infrasound array). The results shown below were accomplished using only option (a) as described above, i.e., an infinite speed was assumed (or equivalently, an instantaneous energy release). In certain altitude regions (where refractive effects are especially large), the detailed propagation path results are quite sensitive to the precise entry speed assigned to the Neuschwanstein bolide. We have
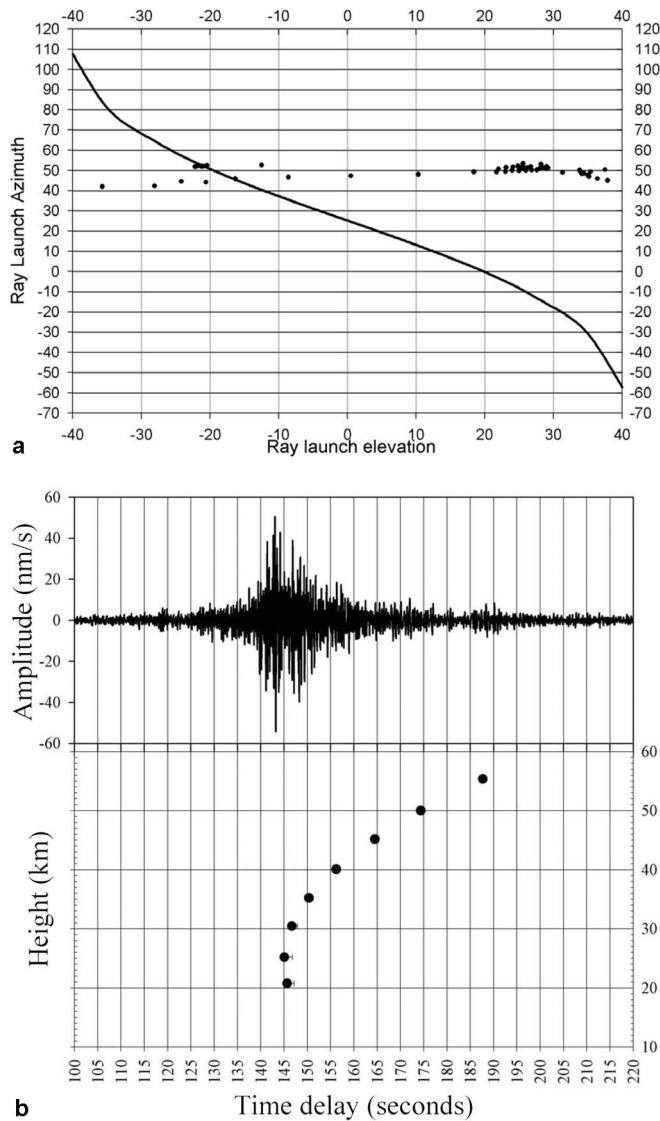
a

b

Fig. 15. a) The azimuth at which modeled rays were launched from the source (along the fireball path) as a function of the modeled ray launch elevation (relative to the horizontal at 0°). Each point represents one ray that is able to reach Freyung from a point along the fireball path. The bold line represents those points that are at right angles to the fireball trajectory; b) the vertical seismic component for station SQTA (top) showing airwave arrival near a time delay of 145 sec. The bottom plot shows the modeled time delays from point sources distributed along the fireball trajectory (as a function of height).

not pursued option (b) fully yet because the computer code that was recently written only accepts a single constant speed over the entire path at the current time and does not have the built-in capability yet to patch together the various sections of the entry trajectory at differing bolide speeds as the body decelerates.

The set of equations used to generate these solutions are identical to those used for the moving point source ray tracing described earlier, but the set of possible launch angles is
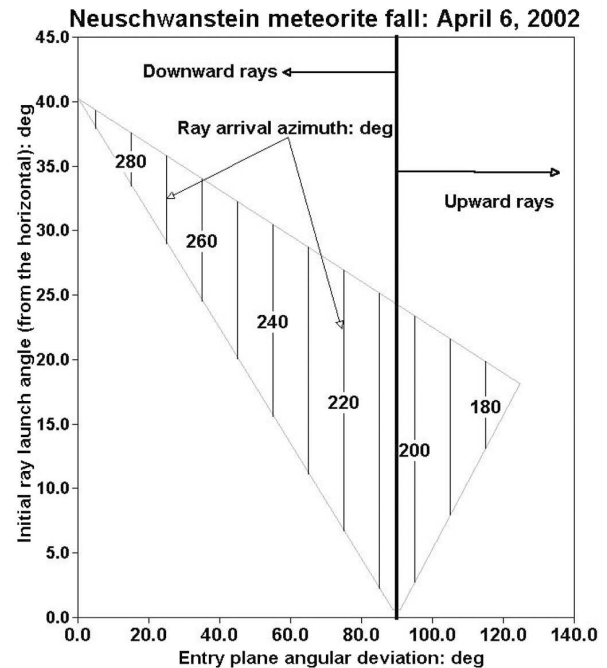

Fig. 16. Initial ray launch angle from the horizontal (°) versus the line source entry plane deviation (°) for Neuschwanstein.

severely restricted by the line source cylindrical geometry, which is, in general, described by a very narrow Mach cone at any height for the range of entry speeds being considered (ignoring fragmentation effects). The line source solution geometry with respect to the Neuschwanstein-Freyung propagation path is given in Fig. 16. From this diagram, using the deduced infrasonic arrival azimuths from 225–234° quoted earlier, we have determined that "rays" would need initially to have been launched downward from the source for entry plane deviations from ~60–70° with initial launch angles of ~8–27°. Our detailed results have been binned into the altitude ranges from 50–80 km and 20–50 km for clarity and are plotted in Figs. 17–22, first for the altitude region of 20–50 km and, subsequently, for the height range of 50–80 km. The respective views that are shown are the top view and the various east-west and north-south side views. The complexity of the detailed propagation paths at great ranges is quite obvious from these figures but especially for source heights along the fireball path above the stratopause. For ranges from ±~50–200 km for this specific entry trajectory, "rays" (actually the local wave normals, which are different from rays when wind effects are properly taken into account) produce an isonified zone on the ground directly below the entry trajectory, while at great ranges, subsequent refraction effects produce distinct zones of silence as well (ignoring diffraction/scattering effects). This effect has been well-known for many years for bolides and for other sources with respect to ground-based sound observations. We have not yet been able to follow the propagation all the way from the source to the receiver for this "line" source type propagation since our computer code
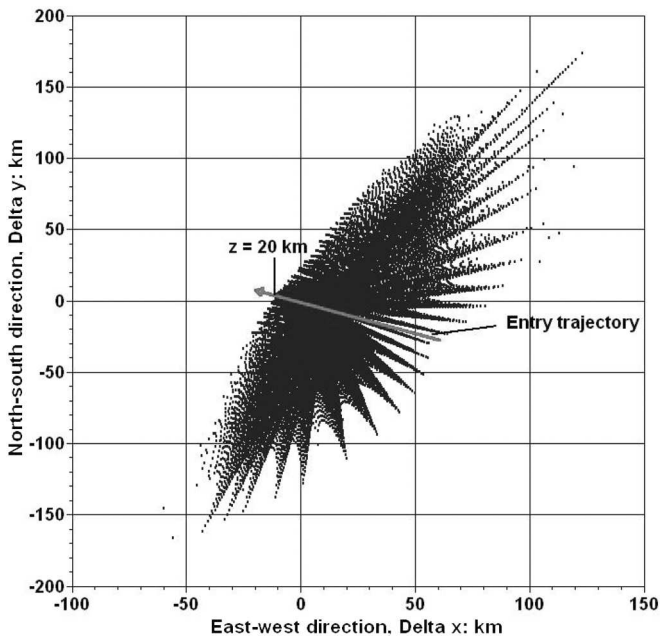
Fig. 17. Top view; line source ray tracing for source altitudes of 20–50 km for Neuschwanstein. Initially downward rays launched at 24 different azimuths for heights 20–50 km at 1 km intervals; V_{inf} = 20.95 km/s is assumed throughout; theta = 49.75°; heading = 295.234°.

Fig. 19. Side view from the east; line source ray tracing for source altitudes of 20–50 km for Neuschwanstein. Initially downward rays launched at 24 different azimuths for heights 20–50 km at 1 km intervals; V_{inf} = 20.95 km/s is assumed throughout; theta = 49.75°; heading = 295.234°.

Fig. 18. Side view from the south; line source ray tracing for source altitudes of 20–50 km for Neuschwanstein. Initially downward rays launched at 24 different azimuths for heights 20–50 km at 1 km intervals; V_{inf} = 20.95 km/s is assumed throughout; heading = 295.234°.

Fig. 20. Top view; line source ray tracing for source altitudes of 50–80 km for Neuschwanstein. Initially downward rays launched at 24 different azimuths for heights 50–80 km at 1 km intervals; V_{inf} = 20.95 km/s is assumed throughout; theta = 49.75°; heading = 295.234°.
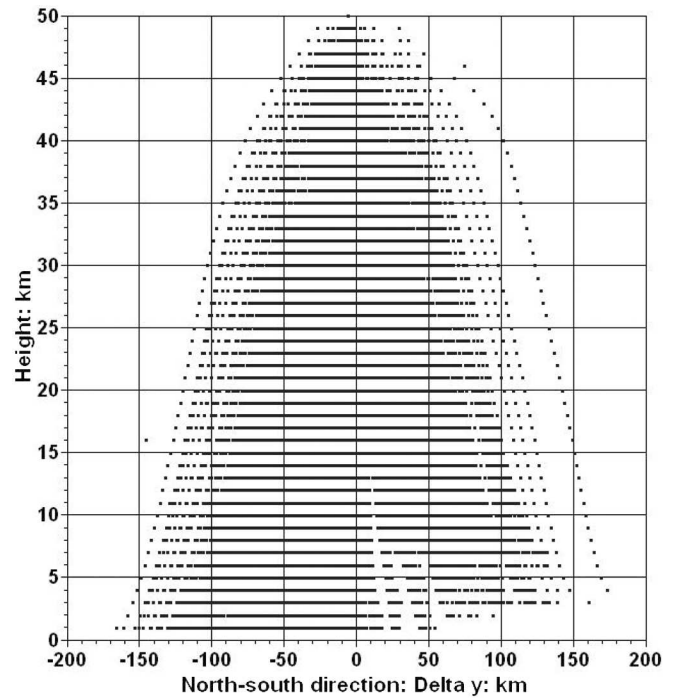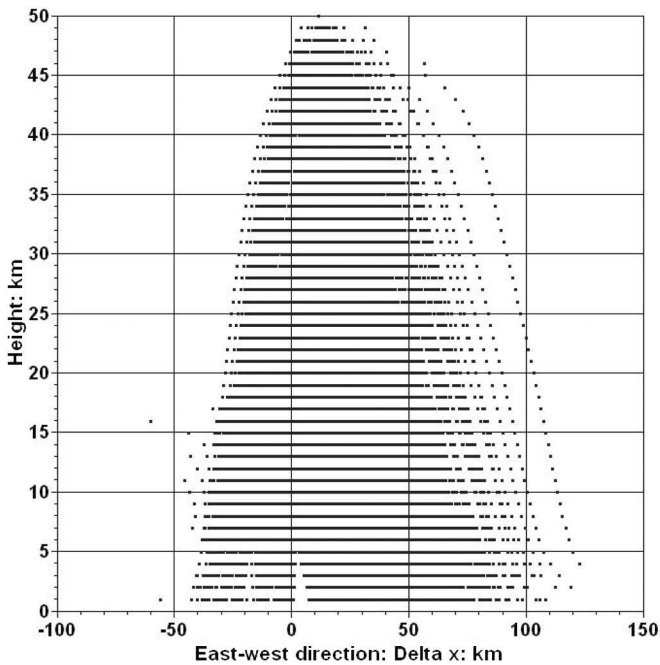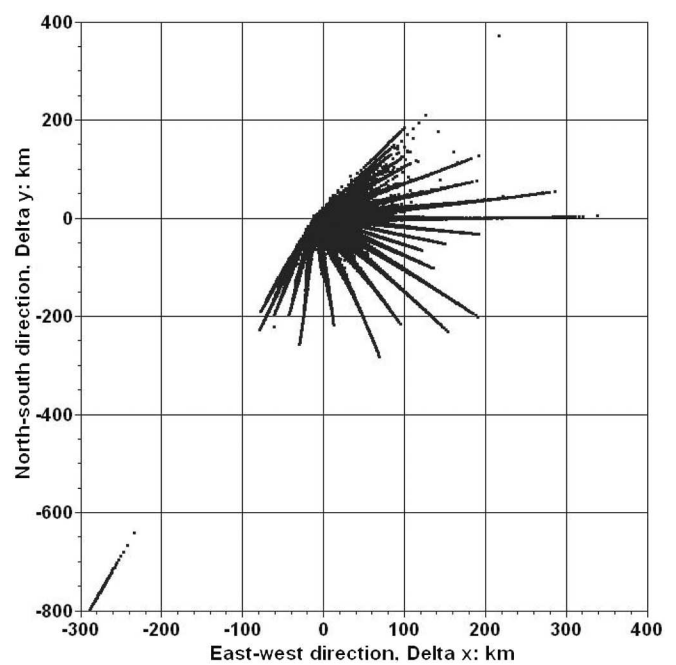
Fig. 21. Side view from the south; line source ray tracing for source altitudes of 50–80 km for Neuschwanstein. Initially downward rays launched at 24 different azimuths for heights 50–80 km at 1 km intervals; V_{inf} = 20.95 km/s is assumed throughout; theta = 49.75°; heading = 295.234°.
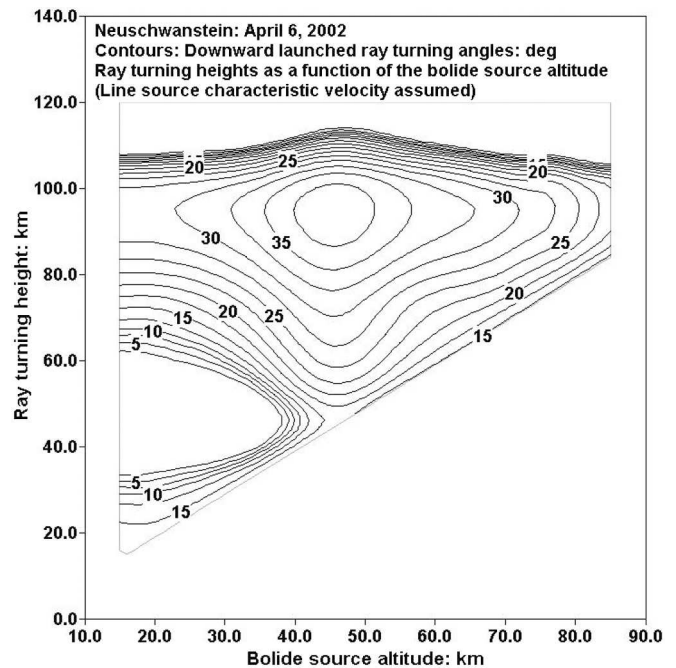
Fig. 23. Contours for downward launched ray turning angles as a function of the line source ray turning height (km) and the source altitude (km) for Neuschwanstein.

has not yet been modified to accomplish this entire task, i.e., it currently only calculates the expected "hypersonic boom carpet." However, we expect that these modifications will soon be accomplished so that the code will be available for future bolide infrasonic and seismic analyses.

Finally, we have also used a simpler ray evaluation code to numerically evaluate the full refractive possibilities for the same set of initial atmospheric (temperature and winds, etc.) and bolide data (heading and entry angles). This additional code does not formally compute the actual ray paths between the source and the receiver but simply calculates the expected turning heights using the same model atmosphere as that used for the moving point and line source ray tracing codes described previously. The results for these calculations are given in Fig. 23 for initially downward rays (see below for more details about the blast radius for Neuschwanstein). These results clearly show turning heights (~40–50 km) below a source height of ~35 km due to atmospheric refractive effects as also seen in the earlier ray tracing results for Neuschwanstein.

Seismic Data

In addition to having been detected infrasonically at Freyung, the airwave from the Neuschwanstein fireball was recorded directly on at least nine seismic stations near the fireball endpoint. Figure 24 shows a ground projection of the fireball and the location of the seismic stations that show an
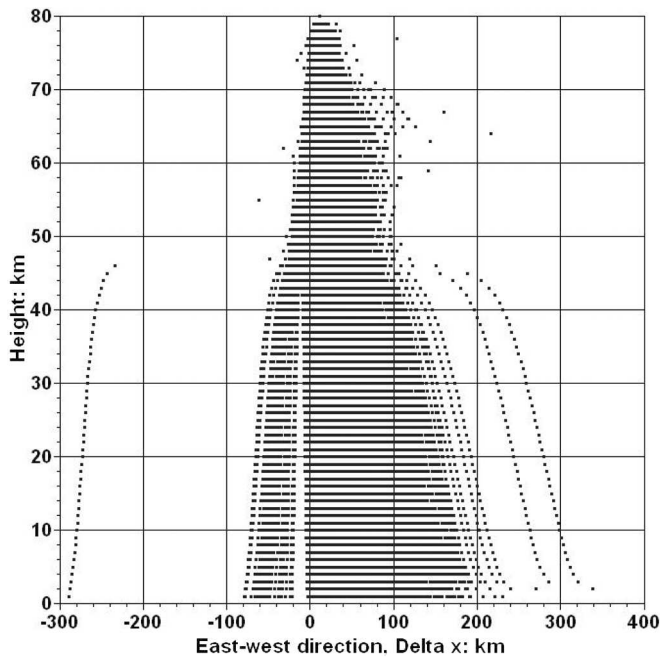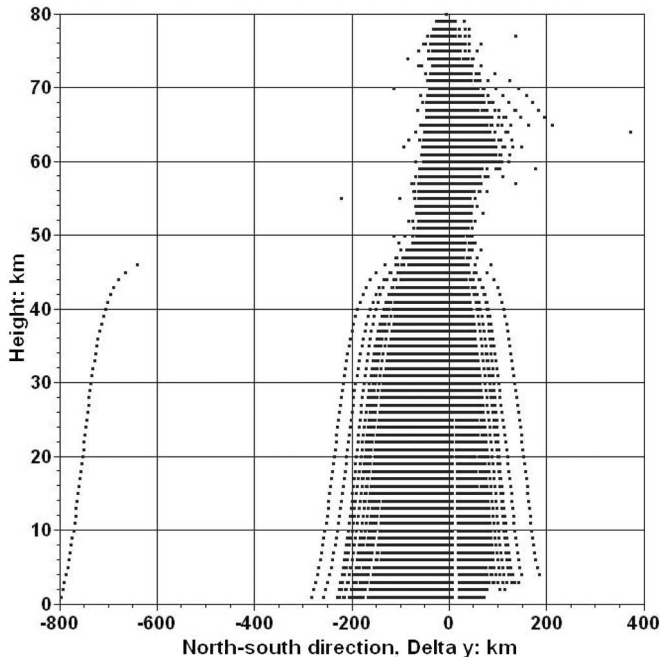

Fig. 22. Side view from the east; line source ray tracing for source altitudes of 50–80 km for Neuschwanstein. Initially downward rays launched at 24 different azimuths for heights 50–80 km at 1 km intervals; V_{inf} = 20.95 km/s is assumed throughout; theta = 49.75°; heading = 295.234°.

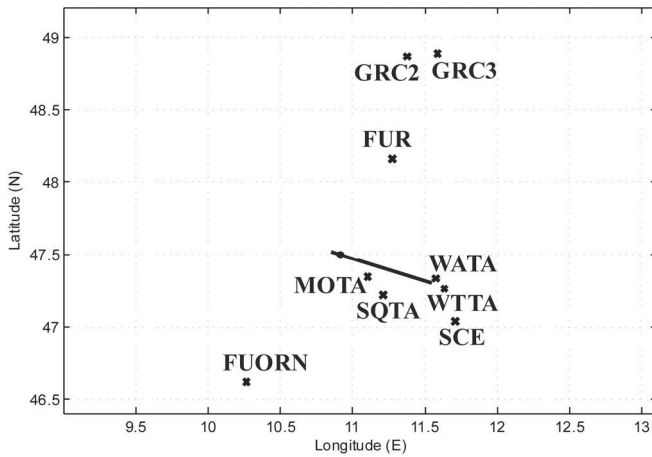Fig. 24. The ground projection of the Neuschwanstein fireball trajectory showing the location of the seismic stations that detected the airwave from the fireball. The point of brightest luminosity is shown as a solid circle symbol.
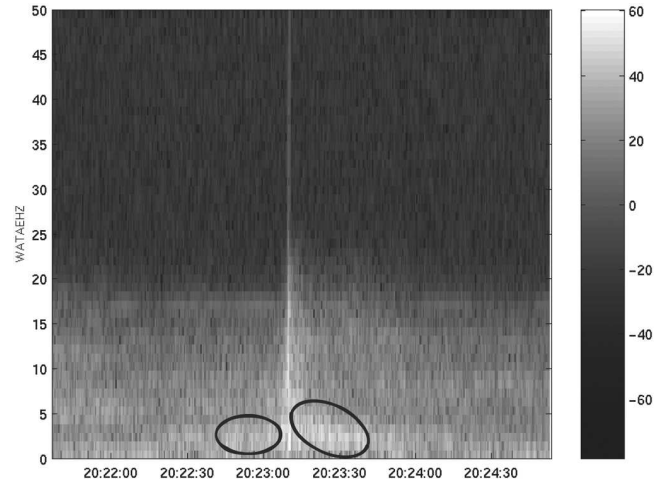

Fig. 25. The signal spectrum associated with the fireball at seismic station WATA. The acoustic wave arrival is represented by the strong, high frequency signal at 20:23:10 UT. The Rayleigh wavetrains immediately before and after this signal are circled in the spectrogram. The ordinate, WATAEHZ, is the measured wave frequency in Hz as a function of the power levels in dB (contoured in black and white).

airwave signal associated with the event. In all cases, these seismic data show the direct expression of the airwave compressing the ground near the seismic station. In addition, acoustically coupled ground waves (Rayleigh) (also commonly called air-coupled Rayleigh waves in the seismic literature) excited proximal to the seismic station are visible as lower frequency precursor signals on some stations. Similarly, several stations show extended Rayleigh wave trains lasting, in some cases, more than a minute after the passage of the main airwave. Similar seismic behavior has been observed previously in the case of the Morávka and Tagish Lake fireballs (cf. Brown et al. 2002a, 2003). Figure 25 shows a spectrogram of the seismic energy for one station, with these different features clearly identifiable.

The character of the signal is different for each station due in part to differences in propagation geometry, source-receiver geometry, instrument sensitivities, and ground properties near the seismographs. Figure 26 shows the vertical component of the raw seismic record (uncorrected for instrumental sensitivity). Table 2 summarizes the seismic stations that recorded signals from the fireball. The time of the arrival of the main acoustic wave and the start and end of the associated Rayleigh wavetrain (if applicable) is summarized in Table 3.

To determine the probable source heights for the acoustic signals recorded at each station, the numerical moving point source ray tracing model used previously to interpret the infrasonic signal at Freyung was again employed. Specifically, rays were shot toward each seismic station (at 5 km increments in height along the fireball trajectory). The same iterative procedure was used again (as with the infrasound signal arrivals at Freyung) to try to determine the azimuth and altitude of any possible acoustical paths that reached the array. In most cases, several paths were found at each specific height. In this way, a series of time delays versus

height along the fireball trajectory were found that could then be compared to the observed airwave arrivals at each station. An example of the procedure is shown in Fig. 15b for one seismic station.

The result of this procedure was to constrain the possible height interval along the fireball path from which the acoustic signal might have been generated. We emphasize that the acoustic path to the station was not restricted to be perpendicular to the fireball trajectory as would be the case for an ideal cylindrical blast source. Rather, we attempted to define any possible accessible acoustic path to the seismic station at each height, irrespective of the source characteristics. The final best-fit source height and allowable height intervals based on the spread in ray arrival times are given in Table 3.

Several stations showed secondary maxima within 5–10 sec of the main airwave arrival. The spectral character of these signals was not similar to the main airwave arrival. However, the most notable secondary events are the later maxima detected at seismic stations: FUR, WTTA, and WATA. And, these are all consistent (based on the ray-trace modeling) with a source near 30 km height along the fireball trajectory. This would be consistent with the smaller signal detected at IS26, which is associated with a possible secondary fragmentation source near a height of 31 km. Alternatively, these secondary events may represent locally enhanced coupling of acoustic energy into Rayleigh waves, possibly as a result of topographical variations or ground character and its lateral variations.

Figure 27 shows the deviation of the ray launch directions from the perpendicular for the best-fit modeled timing for each station. Error margins represent the range of
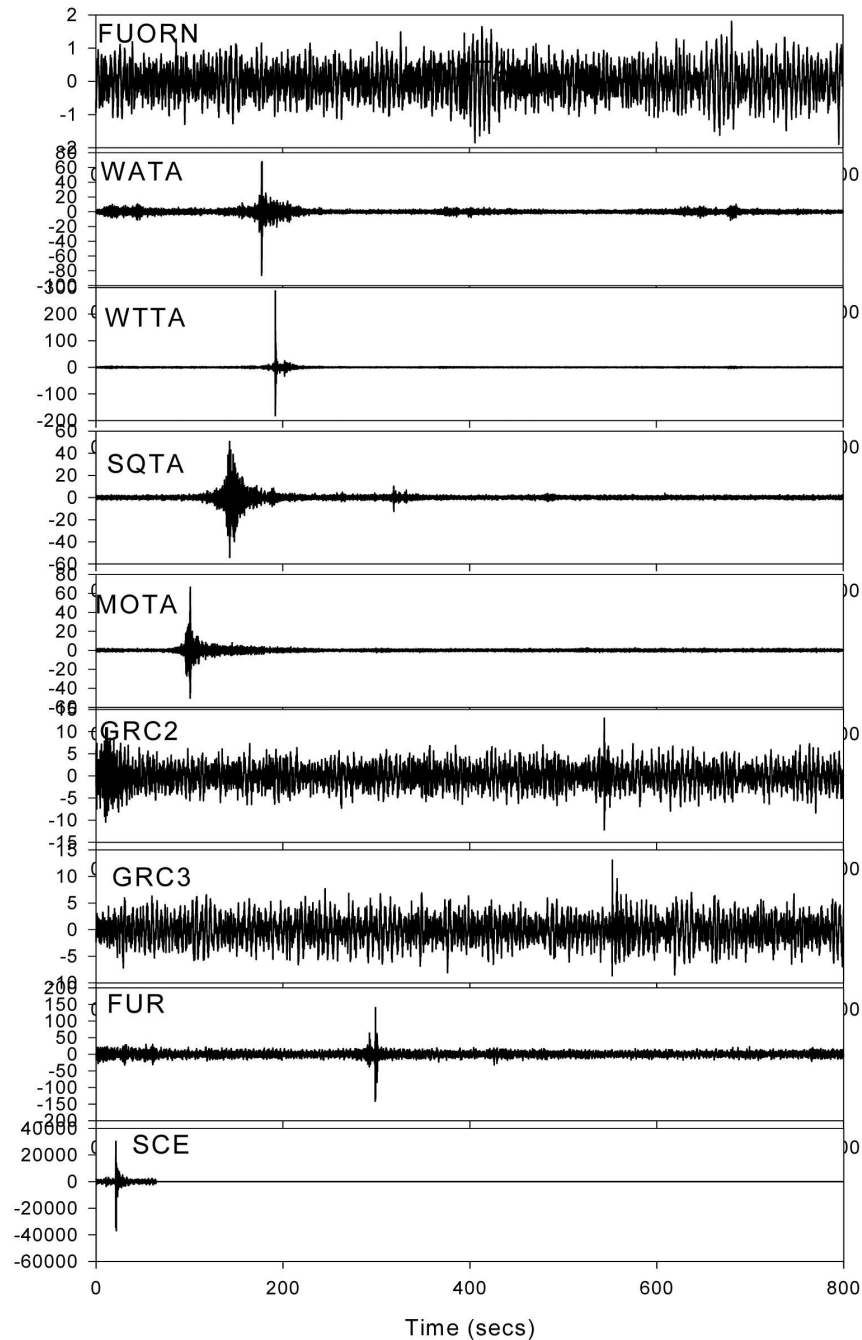
Fig. 26. The raw vertical component of the seismic signals from each station that detected the airwave from the Neuschwanstein fireball. The time is in sec relative to 20:20:13 UT, April 6, 2002. These seismic data have been band-passed to maximize the visibility of the airwave signal; typically, this involves a high-pass filter above 1–2 Hz (depending on the station and local noise characteristics). The signals are uncorrected for seismograph response.

allowable directions given the height intervals where timing matches between the modeled and observed airwave arrivals agreed within the measurable errors. For almost all signals, the deviations are quite small, typically <5°, with error margins allowing deviations possibly as high as 10°. The extreme deviations from the perpendicular launch (and, hence, the possible deviation from line source blast wave geometry) was found to be ~25° in the case of the arrivals at FUORN and FUR. This is very similar to the maximum deviation found for the Morávka fireball event (Brown et al. 2003). It is notable that both seismic stations showed, among the weakest detectable signals, one that is perhaps a reflection of the non-perpendicular geometry involved.

In general, the computed arrivals were systematically 1–

1620 D. O. ReVelle et al.

Table 2. List of seismic stations that detected the Neuschwanstein fireball.

Name	Code	Network	Longitude (°E)	Latitude (°N)	Altitude (m)
Walderalm	WATA	ZAMG-Austria	11.576	47.336	1492
Wattenberg	WTTA	ZAMG-Austria	11.636	47.264	1764
Sankt Quirin	SQTA	ZAMG-Austria	11.209	47.221	1307
Moosalm	MOTA	ZAMG-Austria	11.104	47.345	1575
Ofenpass	FUORN	ZUR-Switzerland	10.26352	46.62022	2333
Gräfenberg Array (Böhmfeld)	GRC2	BGR-Germany	11.376	48.868	447
Fürstenfeldbruck	FUR	FUR-Germany	11.275	48.163	565
Schlegeis	SCE	FUR-Germany	11.7103	47.0386	1737
Gräfenberg Array (Bettbrunn)	GRC3	BGR-Germany	11.586	48.890	445

Table 3. Seismic waves: first arrival times at different stations.

Station	Range[a] (km)	Observed acoustic arrival[b]	C-O res[c] (sec)	R_i[d] (sec)	R_f[d] (sec)	Height[e] (km)	Model launch azimuth[f]	Model launch altitude[f]
MOTA	24	101	4.16	77	197	20 (18–22)	139.83	−43.35
SQTA	36	143	4.16	117	197	25 (20–25)	146.91	−37.9
WATA	38	177.5	1.42	132	227	40 (35–45)	108.36	−42.55
WTTA	41	192.5	2.40	173	213	42 (40–45)	116.66	−43.2
SCE	57	236	4.40	–	249.4	50 (48–52)	137.82	−36.9
FUR	81	299	0.12	–	–	39 (38–41)	4.6	−17.5
FUORN	113	394.5	8.48	–	–	40 (40–45)	220.65	−17.7
GRC2	158	544	2.04	–	–	45 (35–45)	5.65	−2.1
GRC3	164	553	3.72	–	–	40 (35–45)	9.4	8.4

[a]The range is the direct distance between the height of the best-fit (based on the arrival time of the acoustic wave at the seismic station) along the fireball trajectory and each seismic station.

[b]The observed arrival times are in sec relative to 20:20:13 UT on April 6, 2002. The main acoustic arrival has been corrected for the duration of the fireball.

[c]C-O res is the computed-observed residuals in sec.

[d]R_i and R_f are the initial and final times of the observed Rayleigh waves.

[e]The height represents the height along the fireball trajectory that produces the closest time-delay match to the true acoustic arrival based on the ray modeling (see text). The brackets represent the range of possible heights within the modeled range of arrival times.

[f]The model launch azimuth and altitude are the apparent azimuth and altitude of the best-fit rays launched from the fireball trajectory, with negative altitude representing downward directed rays.
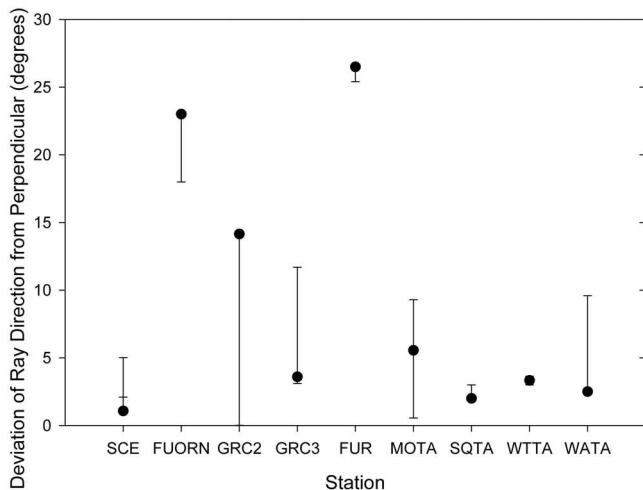
Fig. 27. The deviation of the best-fit ray launch trajectories from the perpendicular for each seismic station. The best-fit solutions were chosen to have the closest arrival match to the observed airwave arrivals (see Table 2). The error margins represent the range of allowed deviations given the spread in modeled arrival timings.

2% later than observed—this strongly suggests that our effective sound velocity was slightly high. However, a path-averaged variation of 1–2% is certainly well within the variability that is expected for effective sound speed (cf. Picone et al. 1997).

The best-fit source regions along the fireball path from our modeling all generally fit into the cylindrical-line source blast wave model, whereby acoustic radiation dominantly emerges perpendicular to the main trajectory. In the case of the nearest stations to the fireball path, MOTA and SQTA, the perpendicular condition was met near the actual fireball endpoint where significant ablation and fragmentation occurred. This undoubtedly contributed to the strong acoustic (and Rayleigh) waves detected at those stations, as we expected a strong acoustic coupling at points of major disruption along the fireball path. All the remaining stations had met perpendicularly at much higher heights along the fireball path; most seem to have detected signals originating from a height of ~40–45 km. Interestingly, the two stations showing the greatest deviation from perpendicular acoustic paths (FUR and FUORN) also have their best-fit source

heights at 39–40 km; this may reflect an enhanced acoustic energy deposition near this altitude that is perhaps associated with an extended zone of low-level fragmentation near this height, though this is a speculative result in the absence of more constraining data (also see the entry dynamics discussion above, where the primary modeled fragmentation processes were initiated at ~23 km to explain the observed bolide panchromatic luminosity).

In general, these seismic data are compatible with most acoustic energy being radiated as part of a cylindrical line source blast wave. Secondary events in the seismic record may be interpreted to support a fragmentation event near 31 km (though not all stations show this secondary event) and, more weakly, an extended zone of possible fragmentation near an altitude of 40 km that was also not seen in the entry dynamics simulations given earlier. However, other results (see below) also suggest source heights near 40–50 km (a possible solution for weak infrasound signals and, alternatively, for the strong infrasound signals, although this latter possibility is far less likely for a number of reasons).

Source Energy Estimation Techniques

We will estimate the energy of Neuschwanstein using a number of observational monitoring (empirical) and modeling techniques, namely, infrasound, seismic, and our entry dynamics modeling approach. In general, we have found that all of these agree at an average initial source energy level of ~<0.02 kt (1 kt = 4.185×10^{12} J). For the entry model, we have determined a best-fit source energy of about 0.0276 kt, compared with an analysis of available flight data that yielded a source energy of 0.0157 kt. For the infrasound data, we have used the following approaches, the first of which is semi-empirical with the latter ones all based on weak shock or linearized wave propagation theory methods (valid at relatively close range where ray methods are applicable; see below for details) and various assumptions about the propagating waves from a blast wave source.

First, from the recorded infrasound data from Neuschwanstein, we have the following parameters as inputs for our calculations (with the measured horizontal range to the bolide = 256 km, with allowable slant ranges of ~260–275 km depending on the assumed source height):

1. First infrasonic wavetrain arrival (estimated earlier at a source height of ~31 km): maximum mean signal amplitude (as noted earlier) = 1.55 ± 0.33 Pa; mean period at maximum signal amplitude = 0.91 ± 0.11 sec.
2. Second infrasonic wavetrain arrival (estimated earlier at a source height of ~22 km): maximum mean signal amplitude (as noted earlier) = 5.36 ± 1.94 Pa; mean period at maximum signal amplitude = 0.35 ± 0.21 sec.

For the sake of simplicity, in the calculations that follow, we used a hydrostatic isothermal, range-independent (perfect stratification) atmospheric model. Since it was clear from other parts of this work that the majority of the infrasound and seismic signals from Neuschwanstein emanated from below ~50 km, we used a mean air temperature of 250.0 K for calculating the constant pressure (density) scale height (=7.317 km) and the constant thermodynamic sound speed (=316.96 m/s) with a constant surface pressure (=1.01325 × 10^5 Pa) as average values over the lowest 50 km in altitude of the middle latitude atmosphere.

First and foremost, for a ray theory type of approach to be valid, the following uniform duct criterion should be satisfied (Ceplecha et al. 1998):

$$R \leq 2 \cdot H^2/\lambda \qquad (1)$$

where H = the vertical duct thickness; λ = the dominant wavelength of the acoustic wave (at maximum signal amplitude) = $\tau \cdot \langle c_s \rangle$; $\langle c_s \rangle$ = the average adiabatic thermodynamic sound speed $\cong$ 0.317 km/s from 0–50 km; τ = the dominant wave period (observed); and R = the distance beyond which wave-guide normal-mode analysis is applicable (rather than ray theory) in interpreting distant signals from blast wave sources. For H = 50 or 100 km, respectively, i.e., for a stratospheric (S) or thermospheric (T) duct with the ground and for λ_{max} = 0.111–0.288 km, R = 17,335 (S) and 69,340 km (T) for the first infrasonic arrival, and R = 45,071 (S) and 180,284 km (T) for the second infrasonic arrival.

Thus, we can safely use a ray theory type, geometrical acoustics approach for all of our analyses below (a summary evaluation of the prediction techniques [a–e]) will be presented in Table 4 below).

a. Observed period at maximum amplitude approach (ReVelle 1997). We have made use of the empirical relationship developed by the AFTAC-Air Force Technical Applications Center, Patrick Air Force Base, Florida, originally developed for much longer range and much larger source energies):

$$\log(E_s/2) = 3.34 \cdot \log(\tau) - 2.58, E_s < 100 \text{ kt} \qquad (2a)$$

or, equivalently:

$$E_s = 2 \cdot (\tau/5.92)^{3.34} \qquad (2b)$$

where E_s = the bolide source energy and τ = the acoustic or infrasonic period at maximum signal magnitude.

b. Line source approach: observed period and slant range including assumed source altitude effects (Ceplecha et al. 1998). This approach assumes that weak shock propagation conditions are applicable throughout the propagation.

$$E_s = (\pi/12) \cdot \rho_m \cdot (\tau/1.579)^4 \cdot (\langle c_s \rangle^7/V) \cdot (1/R) \qquad (3a)$$

$$R_o = k \cdot M \cdot d_m \qquad (3b)$$

where ρ_m = the bolide bulk density; $\langle c_s \rangle$ = the adiabatic, thermodynamic sound speed (height-averaged value); V = the

Table 4. Summary of infrasonic evaluations for Neuschwanstein.

Type of approach	First infrasound arrival: weak[a]	Second infrasound arrival: strong[b]
R_{obs} = 256 km $E_{s\infty}$ = 2.08 × 10^{-2} kt to 2.76 × 10^{-2} kt[c] $E_{s\infty}$ = 1.57 × 10^{-2} kt[d]	τ = 0.91 sec; Δp = 0.775 Pa y = ½ (linear) solution d′ = 1099.4 km	τ = 0.35 sec; Δp = 2.68 Pa y = ¾ (weak shock) solution d′ = 122.3 km
Method a: AFTAC (wave period): E_s[e]	3.84 × 10^{-3} kt	1.58 × 10^{-4} kt
Method b: Line source (wave period): E_s[e]	1.45 × 10^{-3} kt	3.18 × 10^{-5} kt
Method c: Line source (wave amplitude): E_s[e]	1.45 × 10^{-3} kt	3.18 × 10^{-5} kt
Method d: Line source (wave period and amplitude): source height	48.35 km[f]	16.21 km[f]
Method e: Iterative blast wave radius solution for matching observations and theory (see text for details)	Multi-valued solution with heights from ~14.75–15.25 km and 75–83 km for $R_o \cong$ 10–40 m. (See Fig. 8b.)	Multi-valued solution with heights from ~20.5–22.5 and ~38–44 km for $R_o \cong$ 10–40 m. (See Fig. 8a.)

[a] Source altitude search increment = 1.0 km; isothermal, hydrostatic model atmosphere.
[b] Source altitude search increment = 0.50 km; isothermal, hydrostatic model atmosphere.
[c] Entry model source energy estimate (this study; see Table 1 entry dynamics solutions).
[d] Initial source energy estimate of Spurný et al. (2002, 2003).
[e] Bolide source energy at the source height: not the initial bolide kinetic energy.
[f] This source height produces a simultaneous matching of the estimated line source energy using either the amplitude or the period approaches, respectively.

bolide velocity; M = the Mach number = V/c_s; k = the numerical value accounting for break-up effects (with collective wake behavior after break-up, k >1); and R = the slant range from the source to the observer, which was done with no fragmentation effects included (no modifications made in the expression for R_o, i.e., k = 1).

 c. Line source approach: observed amplitude and slant range approach including assumed source altitude effects (Ceplecha et al. 1998).

$$E_s = 11.5 \cdot \pi \cdot \rho_m \ R^3 \ (\Delta p_{o-p} / \sqrt{p_z p_g})^4 (c_s^3 / V) \qquad (4)$$

where p_{o-p} = the pressure amplitude of the acoustic signal (zero to peak value or of the positive phase of the signal); p_z = the ambient pressure at the source generation altitude; and p_g = the ambient pressure at the ground.

 d. Line source approach: observed amplitude and wave period as well as slant range included with the source altitude explicitly calculated to match approach (c) above (ReVelle 1976).

$$\Delta p_{o-p} / \tau = 0.1847 \cdot p^* \cdot (c_s / R) \qquad (5)$$

where p^* = the geometric mean pressure between the source altitude and the ground and $p^* = \sqrt{p_z p_g}$.

 e. New line source approach: differential acoustic efficiency limits.

We have recently performed a total power balance for the Neuschwanstein bolide based on the entry dynamics (including the energetics and fragmentation analyses presented earlier). The full details of this approach will be presented elsewhere since it has just been completed. Briefly, the computation sums up the total power balance of the differential efficiencies of heat, panchromatic light emission (360–675 nm), acoustical waves (through its kinetic energy density), dissociation, and, finally, ionization using a direct scaling relationship between the parameters above and the recently calibrated semi-empirical panchromatic luminous

efficiency of ReVelle and Ceplecha (2001a). In contrast, the differential acoustic efficiency was independently calculated from first principles using blast wave scaling laws and independent, detailed, numerical calculations. Both the differential (and the integral) acoustic efficiency were calculated using the line source blast wave approach given in ReVelle (1976), and the former parameter is used directly in the analysis that follows. We are quite confident that this approach is fundamentally correct because the computed power balance is quite reasonable (summing to nearly 100% over most of the visible bolide trail) and because the differential acoustic efficiency (which is a significant part of the total power balance, especially at low heights) has been calculated totally independent of the other differential efficiencies. Secondly, as will be seen below, the computed theoretical differential acoustic efficiency allows a very reasonable source height estimate to be made for Neuschwanstein (at least for the strongest infrasonic arrivals; see below).

In the following, we have assumed negligibly small dissipative effects, i.e., viscous, thermal, internal molecular relaxation effects, etc. For relatively large bolides such as Neuschwanstein, the fundamental blast wave frequency is sufficiently low that we should expect relatively small dissipative effects, as discussed in ReVelle (1976). This fully justifies our approach at sufficiently low heights (below ~100 km). In our subsequent treatment, we also assumed that the total range to the bolide can be adequately represented by the square root of the square of the horizontal range and of the assumed source height. For close infrasonic detection, this is an acceptable approximation, but at progressively larger ranges, it certainly needs to be examined more carefully, as discussed in ReVelle (1976). In our analysis, we also have neglected the ground reflection factor effect (ReVelle 1976) that should be between unity (no ground reflection) and twice the nominal signal amplitude (if no signal losses due to ground penetration occurred due to a finite ground

impedance). This factor also depends on the elevation arrival angle of the infrasonic signals and cannot simply be evaluated in general. However, as a first step, we have examined the signal doubling limit and found very little detailed change in either of the solutions that were determined below (for the strong and weak infrasonic signals, respectively).

In addition, the solutions determined below were found to be multi-valued in general. This is produced by a combination of effects due to both source height (through the air density) and the total range, which, as discussed above, also includes a source height component. Although the kinetic energy density approach described below is new and incorporates the differential acoustic efficiency for the first time, in essence, it is fundamentally very similar to methods (c) and (d) above. The major difference is that, in what follows below, we have determined the solution numerically and do not use the observed wave frequency to constrain the results. Instead, we have only used the wave frequency to decide whether or not the propagation is in the weakly nonlinear or fully linear domain (through the exponent of the total range to the bolide).

This method interconnects all of the available amplitude data in one iterative approach and numerically matches the observed infrasonic acoustic efficiency at Freyung, within a prescribed tolerance, to the predicted values over a range of possible source heights. A tolerance of 0.1% was assumed over altitude search intervals from 1.0 km (for the weak infrasonic signals) to 0.50 km (for the strong infrasonic signals), respectively. Our entry dynamics results for the initial pre-atmospheric source parameters for Neuschwanstein (mass, velocity, kinetic energy, differential acoustic efficiency) have been least-squares curve-fitted and properly formulated in a new computer code to reliably perform this new numerical approach. The entry model predictions are already known to agree quite well with other independent estimates of the parameters of Neuschwanstein such as ground-based camera and radiometer data, but in general, this new approach will interconnect all of these data, including satellite data, for the first time, in a self-consistent manner. Our new numerical results are presented in Figs. 8a and 8b and are summarized in Table 4.

The fundamental analytical expressions summarizing this type of approach can be written as:

$$\Delta v_o = \Delta v_p(z, x = 10) \cdot f(R) \cdot g(z) \qquad (6a)$$

$$f(R) = ([10.0 \cdot R_o]/R_g)^y = (10.0/x)^y \qquad (6b)$$

$$g(z) = (\rho_o[z = 0]/\rho[z_s])^{1/2} \qquad (6c)$$

and, for an isothermal, hydrostatic atmosphere, Equation 6c can be written in the form:

$$(\rho_{obs}[z = 0]/\rho[z_s])^{1/2} = \exp(z_s/[2H_p]) \qquad (6d)$$

where H_p = constant, and the correction terms for the effects of a non-uniform medium (due to air density changes) are represented above in the function $g(z)$. Slight modifications of the current results are expected for a non-isothermal medium, and these are currently under investigation. The functional relation, $g(z)$ for the air density effects, provides a physical explanation for the nonlinear velocity amplitude growth for wave propagation vertically upward into the atmosphere for a near-ground source such that the wave kinetic energy density is conserved (or, equivalently, the concomitant rapid velocity amplitude decrease for downward wave propagation that results in a rapid evolution toward a linear wave propagation state). The explanation of the y parameter in Equation 6b is given below.

In the expressions above, the symbols are further defined as: z_s = the source height; H_p = the pressure (or density) scale height;

$$H_p \equiv -p(z)/(\partial p[z]/\partial z); \; \partial p(z)/\partial z = -g \cdot \rho$$

R_o = the line source blast wave relaxation radius (ReVelle 1976); R_g = the range at the ground observation point; $x = R/R_o$ = the scaled distance from the source; Δv_o = the observed infrasonic perturbation wind (due to the wave):

$$\Delta v \equiv \Delta p/(\rho \cdot c_s) \qquad (6e)$$

which is written in terms of a locally plane, pressure wave amplitude, Δp, the ambient air density, ρ, and the local sound speed, c_s.

$$\Delta v_p(z, x = 10) = (2.0 \cdot KE_{dp}[z]/\rho[z])^{1/2} \qquad (6f)$$

$\Delta v_p(z, x = 10)$ = the predicted infrasonic perturbation wind; $KE_{dp}(z)$ = the wave kinetic energy density at the source (first defined at $x = 10$).

The perturbation wind due to the wave and its pressure amplitude (see below) is also directly related to the differential acoustic efficiency, $\varepsilon_{theory}(z, x = 10)$, because of our definition:

$$\varepsilon_{theory}(z, x = 10) \equiv KE_{dp}(z)/(KE_{bolide}[z]/V_{ol}[z]) \qquad (6g)$$

$\varepsilon_{theory}(z, x = 10)$ = the wave kinetic energy density/(bolide kinetic energy/source deposition volume); $KE_{bolide}[z]$ = the bolide kinetic energy as a function of height; $V_{ol}[z]$ = the source deposition volume as a function of height:

$$V_{ol} = \pi \cdot R_o^2(z) \cdot l(z) \qquad (6h)$$

defined as energy deposited at $x = 1$; $l(z)$ = line source length.

$$l(z) = \Delta z/\sin\theta \qquad (6i)$$

where θ = the horizontal entry angle of the bolide.

The theoretical differential acoustic efficiency for Neuschwanstein is also available from our entry dynamics results in Fig. 6 in the least-squares, curve-fitted form:

$$\therefore \varepsilon_{theory}(z, x = 10) = 0.9137 \cdot \exp(-0.1609 \cdot z) \qquad (6j)$$

where z is in km and $r^2 = 0.9046495$.

We have also directly computed the theoretical wave kinetic energy density at the source using Equation 6j:

$$KE_{dp}(z) \equiv 1/2 \cdot \rho \cdot (\Delta v_p)^2 = \varepsilon_{theory}(z, x = 10)$$
$$\cdot (KE_{bolide}[z]/V_{ol}[z]) \qquad (6k)$$

Thus, we have changed variables from Equation 6g from the wave kinetic energy density directly to the perturbation wind due to the wave (which was, instead, directly evaluated using either the ground-observed or source height predicted pressure wave amplitude for locally plane waves). This change allowed us to perform iterative calculations to obtain solutions for the possible blast wave radius values as a function of height considered as a free parameter that would allow a self-consistent matching of the predicted and observed wave properties (indicated in Figs. 8a and 8b for the strong and weak infrasonic signals, respectively). The explicit entry dynamics solution for the blast radius as a function of height (including fragmentation effects) is indicated in Fig. 7.

The observed differential acoustic efficiency, ε_{obs}, is also available from the infrasonic data and can be defined as:

$$\varepsilon_{obs} = 1/2 \cdot \rho \cdot (\Delta v)^2/(KE_{bolide}[z]/V_{ol}[z]) = 1/2 \cdot \Delta p^2$$
$$/(\rho \cdot c_{obs}^2)/(KE_{bolide}[z]/V_{ol}[z]) \qquad (6l)$$

with the latter form also written for a locally plane wave so that it could be transformed into the observed pressure wave amplitude.

To calculate the final results, only the numerator of ε_{obs} was necessary since the bolide kinetic energy/deposition volume cancels when the predicted and observed differential acoustic efficiencies are compared in Equation 6a.

The range dependent function in Equation 6b, y, has limits of $y = -3/4$ as $x \to \infty$, respectively, which is the appropriate value for the decay of the pressure (or velocity) amplitude of weakly nonlinear acoustic waves in a uniform medium (ReVelle 1976), or $y = -1/2$ as $x \to \infty$ for "linear," small amplitude waves. To evaluate this possibility in greater detail, we next computed the 10% wave propagation distortion distance for nonlinear wave "steepening" effects to be important (ReVelle 1976), namely:

$$d' = c_s \cdot \tau/(34.3 \cdot \Delta p/p_o) \qquad (6m)$$

If the propagation distance to the observation point is $>d'$, then the wave behavior is deemed linear; otherwise, the weak shock approximation is maintained. For these respective limits in a uniform medium, the parameter, y, can be summarized as:

$y = \frac{1}{2}$ if the propagation is "linear;"
$y = \frac{3}{4}$ if the propagation is weakly nonlinear $\qquad (6n)$

Due to the change in both the observed period at maximum amplitude and the observed maximum pressure amplitude of each of the two infrasonic arrivals for Neuschwanstein, the first infrasonic arrival was predicted to be a linear wave at the observation point, while the second infrasonic arrival was predicted, technically, to have remained a small amplitude weak shock wave during its downward propagation. Note that this prediction in Equation 6m relies not only on a small wave amplitude relative to the ambient value but also on a sufficiently long wave period to achieve wave propagation in a "linearized" state.

Equation 6a resulted directed from the fact that the differential acoustic efficiency at the source, when properly corrected for range and air density variations, should be the same as the observed infrasonic differential acoustic efficiency. Since both of these differential efficiency quantities contain the same divisor, namely, the bolide kinetic energy at any height per unit deposition volume (x = 1), this divisor initially cancels on both sides of Equation 6a. However, to evaluate the theoretical wave kinetic energy density as a function of possible source heights (and, eventually, the perturbation wind due to the wave), the bolide kinetic energy per unit deposition volume as a function of height was needed in combination with the readily available differential acoustic efficiency. This was accomplished by first multiplying the curve fitted $\varepsilon_{theory}(z, x = 10)$ expression for Neuschwanstein by the predicted expression for the bolide's kinetic energy(z)/source deposition volume(z). This later expression was determined by individually curve fitting both the predicted mass, m, and the velocity, V, as a function of height separately and forming the product $\frac{1}{2} m \cdot V^2$. Thus, $KE_{bolide}(z)/V_{ol}(z)$ was ultimately needed for all possible source heights to complete the final computations using all of the variables. The denominator of this latter expression was also determined using a curve fit of the predicted blast wave radius as a function of height (along with a computation of the line source length as well). The final results are slightly sensitive to the assumed threshold acceptance criterion and to the size of the altitude search interval, but the presented results are quite reliable over a range of threshold acceptance values.

Evaluating the expressions above in an iterative manner using the observed horizontal range and for various slant ranges calculated as a function of the source height for an hydrostatic, isothermal atmosphere, we have produced plots of the possible self-consistent values of the nonlinear blast wave relaxation radii solutions that are indicated in Figs. 8a and 8b. Only over a narrow height range of ~20–22 and 38–45 km are the infrasonic observations in agreement with the entry dynamics and other results for the second infrasonic (strong) signal arrival. This is also a similar height range to those deduced earlier, based solely on ray tracing techniques, and to the results found using method (d) above (~16.2 km). For the weaker infrasonic signals, there is much more uncertainty, but a source height of ~15 km and also 75–83 km has been determined using this approach. The lower of these two source heights is probably not very reliable because our curve fit for the predicted kinetic energy of Neuschwanstein is

progressively less accurate below ~18 km. These results do not agree with either the ray tracing results, results observed from the bolide luminous path, or with the approach using Equation 5 listed in Table 4, which will be further examined below.

The source energy plotted in Figs. 8a and 8b was calculated using the expression for the kinetic energy of a spherical non-fragmenting bolide written explicitly in terms of the relaxation blast radius for an ideal line source, namely:

$$E_s = 1/2m \cdot V^2 = ([\pi^{3/2}/2] \cdot [1/(8k^3)] \cdot [1/S_f^{3/2}]) \cdot (\rho_m \cdot Ro^3 \cdot [c_s^3/V]) \tag{6o}$$

where S_f = shape factor, which reduces for a sphere (S_f = 1.209), and where k = 1, i.e., no fragmentation effects (see Equation 3b above) to the standard expression:

$$E_s = (\pi/12) \cdot \rho_m \cdot Ro^3 \cdot (c_s^3/V) \tag{6p}$$

Note that, for k >1 (collective wake behavior), the predicted values of E_s in Figs. 8a and 8b are rapidly reduced further due to the strong dependence on the precise value of k. The value of k is a function of height, however, only over part of the trajectory, i.e., for most purposes, k is essentially unity over a large portion of the entry.

This result is extremely encouraging since it combines for the first time the entry dynamics, the ground-based photographic and radiometer data, and the infrasound/seismic data together in one coherent and self-consistent summary for a bolide. Even satellite data can readily be included in this type of analysis.

DISCUSSION

Given the implications of Neuschwanstein and its connection to the Pribram meteorite fall of April 7, 1959, the importance of its proper modeling and interpretations cannot be overstated. We have determined that the photographic and radiometer evidence, as well as the infrasound and seismic evidence, are all in general agreement about the initial size of this fireball (<0.30–0.33 m or ~400–530 kg for a sphere of <5% uniform volume-weighted porosity or an initial kinetic energy <0.016–0.028 kt.). We have also deduced reliable source heights for the infrasound/seismic signals using both moving point source and line source ray tracing techniques as well as wave propagation methods in an independent manner. At least, for the strongest infrasonic signals, these approaches are in good agreement with one another regarding the altitude range from which these signals emanated. Our source height results can be summarized as follows.

From a moving point-source model using the ray tracing propagation time delay approach, we have ascertained that the weak and strong infrasound signals arrived from ~16–22 km and 30–32 km, respectively. From our new kinetic energy density, wave-amplitude method described in method (e) above, the weak infrasound signals have been found to have

self-consistently arrived from ~15 and from 75–83 km, while the strong infrasound signals were shown to have arrived from possible source heights of 16–22 km and 38–44 km, respectively (multi-valued solution). The former weak infrasound height estimates using method (e) are not very reliable, however, and require further analysis. In addition, from time delay ray tracing analyses using the seismic data alone (see Table 3), we have also independently determined a source height extreme range for the main arrival of 18–52 km, which varies substantially between seismic stations. In addition, there is a secondary maximum seismic time-delay arrival solution with a consistent source height near 30 km. This latter source height has only been determined at a few of the seismic stations but is also in quite reasonable agreement with the moving point-source, ray tracing results determined for the weaker infrasound signals, as described earlier. The majority of all of the height estimates are in general agreement that the ground-based recordings of the original blast wave signals emanated from regions of the trajectory where the brightest luminosity was also measured and where significant fragmentation effects occurred (which is known from the flaring of the light curve), which is a very reassuring feature of our analyses.

CONCLUSIONS

We have produced entry model simulations of the Neushwanstein meteorite fall of April 6, 2002 using the nominal set of entry parameters provided by Spurný et al. (2002, 2003). Very good agreement in source heights, probable dynamics, energetics, and fragmentation behavior has been found using a number of different kinds of data and using a number of fundamentally different techniques. Source energy estimates do not exceed 0.0276 kt, and an average value of ~0.02 kt is in good agreement with that of Spurný et al. (2002, 2003), namely, 0.0157 kt (1 kt = 4.185 × 10^12 J). Moving point source and line source ray tracing techniques have been applied to this case, and generally good agreement between these techniques has been found. Finally, the entry dynamics have been directly connected, using a numerical technique, to the infrasonic and seismic data recorded in association with the entry of Neuschwanstein. Excellent agreement has been found when comparing the ray tracing source height results with the theoretical differential acoustic efficiency numerical results for the strongest infrasonic signals.

Editorial Handling—Dr. Donald Brownlee

REFERENCES

Anglin F. M. and Haddon R. A. W. 1987. Meteoroid sonic shock-wave-generated seismic signals observed at a seismic array. *Nature* 328:607–609.

Arase T. 1959. Some characteristics of long-range explosive sound propagation. *The Journal of the Acoustical Society of America* 31:588–595.

Beer T. 1974. *Atmospheric waves.* New York: Halsted Press. 315 p.

Borovička J. and Kalenda P. 2003. The Morávka meteorite fall: 4. Meteoroid dynamics and fragmentation in the atmosphere. *Meteoritics & Planetary Science* 38:1023–1045.

Borovička J., Spurný P., Kalenda P., and Tagliaferri E. 2003a. The Morávka meteorite fall: 1. Description of the events and determination of the fireball trajectory and orbit from video records. *Meteoritics & Planetary Science* 38:975–989.

Borovička J., Weber H. W., Jopek T., Jakes P., Randa Z., Brown P. G., ReVelle D. O., Kalenda P., Schultz L., Kucera J., Haloda J., Týcová P., Frýda J., and Brandstätter F. 2003b. The Morávka meteorite fall: 3. Meteoroid initial size, history, structure, and composition. *Meteoritics & Planetary Science* 38:1005–1021.

Brown P., ReVelle D. O., Tagliaferri E., and Hildebrand A. R. 2002a. An entry model for the Tagish Lake fireball using seismic, satellite, and infrasound records. *Meteoritics & Planetary Science* 37:661–676.

Brown P., Spalding R. E., ReVelle D. O., Tagliaferri E., and Worden S. P. 2002b. The flux of small near-Earth objects colliding with the Earth. *Nature* 420:294–296.

Brown P., Whitaker R. W., and ReVelle D. O. 2002c. Multi-station infrasonic observations of two large bolides: Signal interpretation and implications for monitoring of atmospheric explosions. *Geophysical Research Letters* 29:1–4.

Brown P. G., Kalenda P., ReVelle D. O., and Borovička J. 2003. The Morávka meteorite fall: 2. Interpretation of infrasonic and seismic data. *Meteoritics & Planetary Science* 38:989–1003.

Ceplecha Z., Borovička J., Elford W. G., ReVelle D. O., Hawkes R. L., Porubčan V., and Šimek M. 1998. Meteor phenomena and bodies. *Space Science Reviews* 84:327–471.

Cevolani G. 1994. The explosion of the bolide over Lugo di Romagna (Italy) on 19 January 1993. *Planetary and Space Science* 42:767–775.

Cumming G. L. 1989. Alberta bolide of June 1, 1982: Interpretation of photographic and seismic records. *Canadian Journal of Earth Sciences* 26:1350–1355.

Evers L. and Haak H. 2001. Sounds from a meteor and oceanic waves. *Geophysical Research Letters* 28:41–44.

Folinsbee R. E., Bayrock L. A., Cumming G. L., and Smith D. G. W. 1969. Vilna meteorite: Camera, visual, seismic, and analytic records. *Journal of the Royal Astronomical Society of Canada* 63:61–86.

Halliday I., Blackwell A. T., and Griffin A. A. 1990. Evidence for the existence of groups of meteorite-producing asteroidal fragments. *Meteoritics & Planetary Science* 25:93–99.

Hedin A. E., Fleming E. L., Manson A. H., Schmidlin F. J., Avery S. K., Clark R. R., Franke S. J., Fraser G. J., Tsuda T., Vial F., and Vincent R. A. 1996. Empirical wind model for the upper, middle, and lower atmosphere. *Journal of Atmospheric and Terrestrial Physics* 58:1421–1447.

Ishihara Y., Tsukada S., Sakai S., Hiramatsu Y., and Furumoto M. 2001. Determination of the fireball trajectory using dense seismic arrays. *Bulletin of the Earthquake Research Institute* 76:87–92.

McIntosh B. A. and ReVelle D. O. 1984. Traveling atmospheric pressure waves measured during a solar eclipse. *Journal of Geophysical Research* 89:4953–4962.

Picone J. M., Hedin A. E., Coffey S. L., Lean J., Drob D. P., Neal H., Melendez-Alvira D. J., Meier R. R., and Mariska J. T. 1997. The Naval Research Laboratory program on empirical models of the neutral upper atmosphere. In *Astrodynamics 1997: Advances in astronautical sciences,* edited by Hoots F. R., Kaufman B., Cefola P. J., and Spencer D. B. San Diego: American Astronautical Society. pp. 515–528.

Qamar A. 1995. Space Shuttle and meteoroid-tracking supersonic objects in the atmosphere with seismographs. *Seismological Research Letters* 66:6–12.

ReVelle D. O. 1976. On meteor-generated infrasound. *Journal of Geophysical Research* 81:1217–1240.

ReVelle D. O. 1997. Historical detection of atmospheric impacts of large super-bolides using acoustic-gravity waves. *Annals of the New York Academy of Sciences* 822:284–302.

ReVelle D. O. 2001. Theoretical Leonid entry modeling. In *Proceedings of the Meteoroids 2001 Conference,* edited by Warmbein B. ESA SP-495. Noordwijk: European Space Research and Technology Center. pp. 149–154.

ReVelle D. O. 2002a. Fireball dynamics, energetics, ablation, luminosity, and fragmentation modeling. In *Proceedings of the Conference Asteroids, Comets, Meteors (ACM 2002),* edited by Warmbein B. ESA SP-500. Noordwijk: European Space Research and Technology Center. pp. 127–136.

ReVelle D. O. 2002b. Porosity: A natural alternative explanation of bolide types, their atmospheric behavior and the implications. In *Proceedings of the Conference Asteroids, Comets, Meteors (ACM 2002),* edited by Warmbein B. ESA SP-500. Noordwijk: European Space Research and Technology Center. pp. 233–236.

ReVelle D. O. and Ceplecha Z. 2001a. Bolide physical theory with application to PN and EN fireballs. In *Proceedings of the Meteoroids 2001 Conference,* edited by Warmbein B. ESA SP-495. Noordwijk: European Space Research and Technology Center. pp. 507–512.

ReVelle D. O. and Ceplecha Z. 2001b. Calculations of shape change and fragmentation parameters using very precise bolide data. In *Proceedings of the Meteoroids 2001 Conference,* edited by Warmbein B. ESA SP-495. Noordwijk: European Space Research and Technology Center. pp. 551–556.

Spurný P., Heinlein D., and Oberst J. 2002. The atmospheric trajectory and heliocentric orbit of the Neuschwanstein meteorite fall on April 6, 2002. In *Proceedings of the Conference Asteroids, Comets, Meteors (ACM 2002),* edited by Warmbein B. ESA SP-500. Noordwijk: European Space Research and Technology Center. pp. 137–140.

Spurný P., Oberst J., and Heinlein D. 2003. Photographic observations of Neuschwanstein: A second meteorite from the orbit of the Príbram chondrite. *Nature* 423:151–153.